UNIVERSITÀ
DI PAVIA

Dipartimento di Medicina Molecolare

# Genetic characterization and genotype-phenotype correlation of cerebellar and brainstem congenital defects

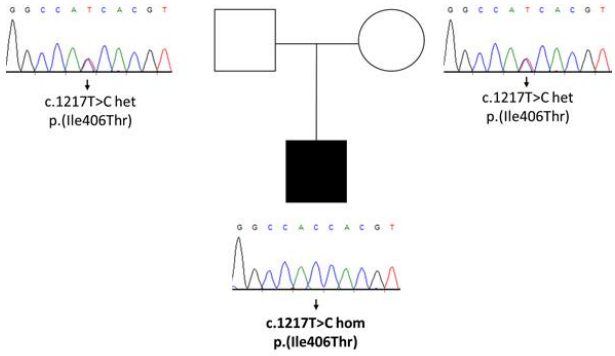


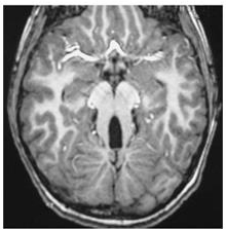

**Monia Ginevrino**

Dottorato di Ricerca in
Genetica, Biologia Molecolare e Cellulare
Ciclo XXXII – A.A. 2016-2019

UNIVERSITÀ
DI PAVIA

Dipartimento di Medicina Molecolare

# Genetic characterization and genotype-phenotype correlation of cerebellar and brainstem congenital defects

**Monia Ginevrino**

**Supervised by Prof. Enza Maria Valente**

Dottorato di Ricerca in
Genetica, Biologia Molecolare e Cellulare
Ciclo XXXII – A.A. 2016-2019

*To my mother*
*Wish you were here…*

## *Abstract*

Cerebellar and Brainstem Congenital Defects (CBCDs) encompass a group of congenital malformations resulting from an alteration of the brain development. These developmental anomalies are genetically and phenotypically heterogeneous. Through a Next Generation Sequencing approach, a big cohort of CBCD patients has been analyzed with the aim to improve genotype-phenotype correlations to better understand the genetic bases of these disorders, as well as to expand current knowledge through the identification of new candidate genes. Pathogenic variants have been identified in 59% patients with Joubert Syndrome (264 out of 444), and in 67% children with Pontocerebellar hypoplasia (43 out of 64). Other CBCDs phenotypes include (percentage of solved cases in brackets): 2 Horizontal Gaze Palsy with Progressive Scoliosis (100%); 15 Poretti-Boltshauser Syndrome (93%); 6 Whole Cerebellar Hypoplasia (33%); 28 Nonprogressive Congenital Ataxia (7%). Four new candidate genes have been identified (*SUFU*, *GSX2*, *TTL*, and *FSD1L*) and phenotypic expansion has been performed for *SPTBN2*, *BRAT1*, *KIF1A* and *IRF2BPL* genes. In conclusion, Next Generation sequencing is a powerful technique for the characterization of genetically heterogeneous conditions such as CBCDs and for the identification of still uncovered causative genes.

# *Abbreviations*

1000G: 1000 Genomes
BPC: Blake pouch cyst
CADD: Combined Annotation Dependent Depletion
CBCDs: Cerebellar and Brainstem Congenital Defects
CCM: Cerebellar Congenital Malformations
cDNA: Complementary Dessossiribonucleic Acid
CGH: Comparative Genomic Hybridization
CNS: Central Nervous System
CNVs: Copy Number Variations
dbSNP: Single Nucleotide Polymorphism Database
DNA: Desossiribonucleic Acid
dNTPs: Deoxynucleotides Triphosphate
DQ: Dosage Quotient
dsDNA: Double Strand Deossirobonucleotide
DWM: Dandy-Walker Malformation
EEG: Electroencephalogram
EVS: Exome Variant Server
GERP: Genomic Evolutionary Rate Profiling
GnomAD: Genome Aggregation Database
GTEx: Genotype-Tissue Expression
HGMD: Human Gene Mutation Database
HGPPS: Horizontal Gaze Palsy with Progressive Scoliosis
INAD: Infantile Neuroaxonal Dystrophy
iPSCs: Induced Pluripotent Stem Cell
JS: Joubert Syndrome

KO: Knock-out

lncRNA: Long Noncoding RNA

MAF: Minor Allele Frequency

MCDs: Malformations of Cortical Development

MCM: Mega Cisterna Magna

MLPA: Multiplex Ligation-dependent Probe Assay

MRI: Magnetic Resonance Imaging

NGS: Next Generation Sequencing

NPCA: Nonprogressive Congenital Ataxia

PCH: Pontocerebellar Hypoplasia

PCR: Polymerase Chain Reaction

PEST: Proline (P), glutamic acid (E), serine (S), and threonine (T)

PFAC: Posterior Fossa Arachnoid Cyst

PTCD: Pontine Tegmental Cap Dysplasia

RMFSL: Rigidity and Multifocal Seizure Syndrome

RNA: Ribonucleic Acid

RT: Reverse Transcription

RT-PCR: Real Time Polymerase Chain Reaction

SCA5: Spinocerebellar Ataxia 5

SCAR14: Spinocerebellar Ataxia, Autosomal Recessive 14

SHH: Sonic-Hedgehog Homolog

SIFT: Sorting Intolerant From Tolerant

SNV: Single Nucleotide Variant

VACTERL: Vertebral defects, Anal atresia, Cardiac defects, Tracheo-Esophageal fistula, Renal anomalies, and Limb abnormalities

WES: Whole Exome Sequencing

# Contents

*Abstract* ..... 4
*Abbreviations* ..... 5
*Contents* ..... 7
1. Introduction ..... 9
2. CBCDs classification ..... 13
Predominantly cerebellar malformations ..... 14
Dandy-Walker Malformation ..... 14
Rhombencephalosynapsis ..... 15
Cerebellar hypoplasia ..... 15
Isolated vermis hypoplasia ..... 17
Cerebellar hyperplasia ..... 18
Cerebellar dysplasia and cerebellar cysts ..... 18
Cerebellar and brainstem malformations ..... 20
Pontocerebellar hypoplasia ..... 20
Tubulinopathies ..... 23
Alpha-dystroglycanopathies ..... 23
Joubert syndrome ..... 24
Other rare CBCDs ..... 28
Predominantly brainstem malformations ..... 30
Pontine Tegmental Cap Dysplasia ..... 30
Horizontal Gaze Palsy with Progressive Scoliosis ..... 30
Diencephalic-mesencephalic junction dysplasia ..... 30
3. Aims of the research ..... 32
4. Materials and methods ..... 33
Sample preparation ..... 33
Next Generation Sequencing ..... 34
Bioinformatic analysis ..... 36
Sanger sequencing ..... 38
Multiplex Ligation-dependent Probe Assay ..... 39
Real time PCR ..... 40
5. Results ..... 41
Custom Target Resequencing ..... 41

Joubert syndrome ..... 41
Pontocerebellar hypoplasia ..... 42
Other CBCDs ..... 44
SPTBN2 ..... 44
Whole Exome Sequencing ..... 47
SUFU ..... 47
GSX2 ..... 49
TTL ..... 51
IRF2BPL ..... 53
KIF1A ..... 55
BRAT1 ..... 56
FSD1L ..... 59
6. Discussion ..... 66
7. Conclusions and perspectives ..... 75
*References* ..... 77
*Supplementary tables* ..... 83
*List of original manuscripts* ..... 99

# 1. Introduction

The cerebellum arises from the dorsal anterior portion of the hindbrain, one of the segments of the neural tube with midbrain, forebrain and spinal cord. It is connected to the brainstem through the cerebellar peduncles (superior, middle and inferior) and consists macroscopically of two symmetric cerebellar hemispheres connected medially by the cerebellar vermis. The cerebellar tissue is organized in an onion-like aspect, with the cerebellar folia running parallel to the calvarium (Figure 1). Main functions controlled by the cerebellum are balance, muscular tone and posture, coordination, but the cerebellum also plays a major role in cognition. The brainstem is characterized by the midbrain and by pons and medulla oblongata, which originate from the posterior portion of the hindbrain. An important role of the brainstem consists in the control of the flow messages between the brain and the rest of the body. Moreover, it represents the origin of the cranial nerves III and IV and regulates breathing, heart rate, blood pressure, consciousness, sleep-wake cycle.

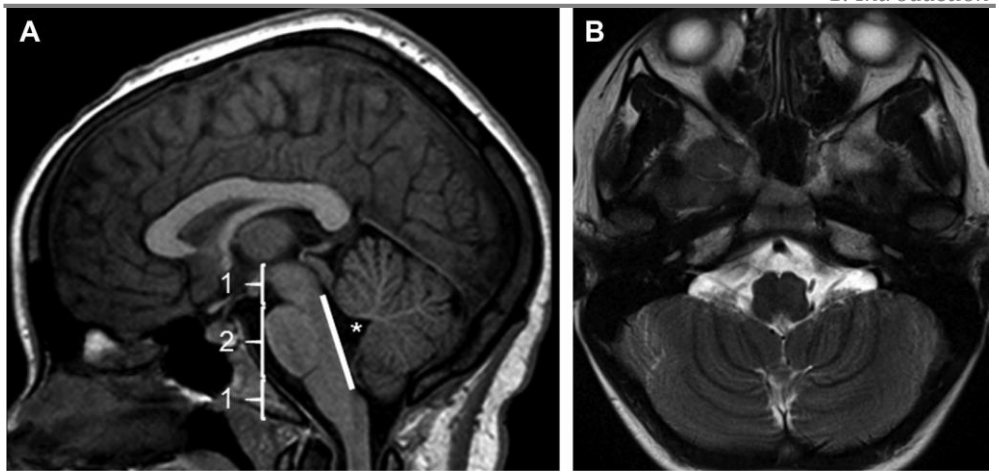


**Figure 1**. Normal anatomy of cerebellum and brainstem. (A) MRI showing the right proportions of the brainstem: rostrocaudal length of the pons is approximately twice [2] with respect to the midbrain [1] and medulla [1]), the white line indicates a flat dorsal surface of the brainstem, while the asterisk shows the normal position of the fastigium, below the midpoint of the ventral pons. (B) MRI showing the normal orientation of the cerebellar folia (onionlike orientation) (Poretti et al. 2016).

Cerebellar and Brainstem Congenital Defects (CBCDs) are a heterogeneous group of malformations of the posterior cranial fossa caused by defects of the brain development and characterized by high phenotypic variability and genetic heterogeneity. These alterations can be caused by pathogenic gene variants, teratogens, or a combination of both (Poretti et al. 2016). Typical signs of cerebellar involvement, such as ataxia, hypotonia and nystagmus, can be accompanied by other symptoms, including developmental delay, intellectual disability, behavioral disturbances (including autistic traits) and variable

multiorgan involvement (Barkovich et al. 2009; Doherty et al. 2013). More severe symptoms that can occur comprise abnormalities of the breathing pattern, dysphagia and dysarthria, spasticity and seizures. The incidence of CBCDs is not yet well defined, but an overall prevalence of 1.30 per 100,000 births has recently been estimated for cerebellar hypoplasia, with or without other CNS malformations (Howley et al. 2018). Another estimate, concerning mainly Dandy-Walker malformation in Europe, reported a prevalence of 2.74:100,000 (Santoro et al. 2019); in contrast with the previously reported global interval of 1:30,000-1:5,000 births (Doherty et al. 2013).

In most cases, the diagnosis of CBCD can be suspected prenatally by ultrasound in the second trimester of gestation (Forzano et al. 2007). When not identified during pregnancy, a congenital malformation of the posterior fossa can be ascertained postnatally through magnetic resonance imaging (MRI). Recent advances in genetic and neuroimaging have led great improvement in the knowledge of CBCDs. Moreover, the study of animal models such as mouse, chicken and zebrafish has been precious for the understanding of mechanisms underlying cerebellar and brainstem embryonic development (Doherty et al. 2013). However, many aspects of CBCDs are currently unclear, such as the implications of these malformations on cognitive, behavioral and neuro-ophthalmological development, as well as mortality rate and life expectancy (Barkovich et al. 2009). A long-term neurological outcome study on congenital cerebellar malformations has recently shown that neurodevelopmental deficits

are more severe if the malformation involves the brainstem or cerebellar hemispheres, while children with vermis hypoplasia seem less likely to have global developmental delay (Pinchefsky et al. 2019). These anomalies are mainly caused by genetic alterations inherited in an autosomal recessive or X-linked manner, nevertheless, an increasing number of sporadic conditions caused by *de novo* pathogenic variants are emerging (Doherty et al. 2013). Moreover, chromosomal rearrangements including translocations, deletions and duplications are causative for some types of CBCD (for instance, Dandy-Walker Syndrome) (Grinberg et al. 2004).

# 2. CBCDs classification

A proper and detailed classification of CBCDs is important as it can guide the diagnosis and, consequently, it can provide information concerning the prognostic implications and recurrence risk. Moreover, the identification of a genetic cause is important for prenatal test, preimplantation genetic diagnosis and carrier screening. To date different classification models have been proposed. The first classification scheme was based on the molecular and cellular mechanisms that regulate embryonic development of the central nervous system (Barkovich et al. 2009). Subsequently, a classification model based on molecular genetics and neuroradiological characteristics (and thus considering mainly the malformative aspect) has been proposed and universally adopted (Bosemani et al. 2015; Doherty et al. 2013; Jissendi-Tchofo et al. 2015; Poretti et al. 2016). According to this classification, CBCDs can be grouped in three classes: predominantly cerebellar malformations, cerebellar and brainstem malformations, predominantly brainstem malformations.

## Predominantly cerebellar malformations

### *Dandy-Walker Malformation*

The most frequent posterior fossa anomaly, DWM is characterized by hypoplasia of the cerebellar vermis which is upward rotated and elevated and by a cystic dilatation of the fourth ventricle. Moreover, cerebellar hemispheres are also hypoplastic and moved anterolaterally and the size of the posterior fossa is enlarged. Additional malformations can be present; in particular, hydrocephalus is present in 90% of children with DWM. This malformation occurs sporadically and can be isolated or part of other syndromes (Poretti et al. 2016). Some chromosomal rearrangements have been correlated with DWM (6q24 deletion, 9p duplication, 13q2 deletion, 2q36 deletion) as well as rare and still unconfirmed alterations in six genes (*ZIC1*, *ZIC4*, *FOXC1*, *FGF17*, *LAMC1*, and *NID1*) (Bosemani et al. 2015).

Other cystic malformations are represented by Blake pouch cyst (BPC), mega cisterna magna (MCM) and posterior fossa arachnoid cyst (PFAC). Differences with DWM are summarized in Table 1.

**Table 1.** Differences between cystic malformations of the CNS

| ***Disease*** | ***Vermis size*** | ***IV ventricle size*** | ***Posterior fossa size*** | ***Hydrocephalus*** |
|---|---|---|---|---|
| *DWM* | Hypoplastic | Enlarged | Enlarged | Yes (90% of patients) |
| *BPC* | Normal | Enlarged | Normal | Yes |
| *MCM* | Normal | Normal | Inconsistently enlarged | No |
| *PFAC* | Normal | Normal or reduced | Normal | Possible |

### *Rhombencephalosynapsis*

Rhomboencephalosynapsis is a sporadic condition with a low recurrence risk characterized by partial or complete absence of the cerebellar vermis with the consequent fusion of the cerebellar hemispheres. Often, this malformation is associated with other syndromes (Gòmes-Lòpez-Hernàndez syndrome and VACTERL syndrome) and may be accompanied by other CNS anomalies such as hydrocephalus and holoprosencephaly (Bosemani et al. 2015). No genetic correlation has been yet found.

### *Cerebellar hypoplasia*

Most of the cases of cerebellar hypoplasia (reduced-size cerebellum) do not have a genetic cause identified so far. However, pathogenic variants in *OPHN1* are responsible for an X-linked recessive form of

cerebellar hypoplasia with ventriculomegaly, intellectual disability, epilepsy and mild dysmorphic facial features.

Cerebellar hypoplasia / atrophy is also a hallmark in a clinically and genetically heterogeneous group of disorders called *"Nonprogressive congenital ataxias"* (NPCA). The main feature of these conditions is represented by lack of progression of the typical cerebellar symptoms; in contrast, a clinical improvement is often observed. MRI can range from normal to patterns of cerebellar hypoplasia or nonprogressive cerebellar atrophy (enlargement of interfolial spaces; condition known as "Shrunken cerebellum") and only rarely a progressive enlargement of the cerebellar fissures is observed (Bertini et al. 2018). Dominant, recessive, and X-linked inheritance has been described for these disorders. Known NPCA genes are listed in Table 2.

**Table 2.** NPCA genes with their respective inheritance model and cytogenetic location (Bertini et al. 2018; Zanni et al. 2018).

| *Gene* | *Inheritance* | *Cytogenetic location* |
|---|---|---|
| CACNA1A | AD | 19p13.13 |
| KCNC3 | AD | 19q13.33 |
| ITPR1 | AD | 3p26.1 |
| VLDLR | AR | 9p24.2 |
| WDR81 | AR | 17p13.3 |
| CA8 | AR | 8q12.1 |
| ATP8A2 | AR | 13q12.13 |
| PMPCA | AR | 9q34.3 |
| WWOX | AR | 16q23.1-q23.2 |
| GRM1 | AD/AR | 6q24.3 |
| SPTBN2 | AD/AR | 11q13.2 |
| KCNJ10 | AR | 1q23.2 |
| KIAA0226 | AR | 3q29 |
| GRID2 | AR | 4q22.1-q22.2 |
| WDR73 | AR | 15q25.2 |
| CAMTA1 | AD | 1p36.31-p36.23 |
| ATCAY | AR | 19p13.3 |
| ATG5 | AR | 6q21 |
| ATP2B3 | XLR | Xq28 |
| ABCB7 | XLR | Xq13.3 |
| ATP7A | XLR | Xq21.1 |

AD, autosomal dominant; AR, autosomal recessive; XLR, X-linked recessive

### *Isolated vermis hypoplasia*

Often wrongly called “Dandy-Walker variant”, isolated vermis hypoplasia is a partial absence of the inferior portion of the cerebellar vermis. Other posterior fossa structures are normal, and the outcome

is usually favorable. Some patients may show receptive language and mild functional deficits in fine motor activity.

### *Cerebellar hyperplasia*

Cerebellar hyperplasia (macrocerebellum) consists in an increased size of the cerebellum without morphological or signal abnormalities. It can be an isolated neuroradiological finding or it may be part of a variety of syndromes (such as Sotos syndrome, Costello syndrome, mucopolysaccharidoses and fucosidosis). The genetic background underlying this condition is currently unknown and the phenotypic expression is highly variable.

### *Cerebellar dysplasia and cerebellar cysts*

Cerebellar dysplasia consists in a disorganization of the cerebellar tissue as a result of an abnormal foliation and fissuration during the embryonic development. This condition may be asymptomatic or cause a severe neurologic impairment. A cerebellar dysplasia with known genetic cause is the Chudley-McCullough syndrome, caused by recessive pathogenic variants in *GPSM2*. Other conditions are characterized by the presence of cerebellar cysts and include: *GPR56*-related polymicrogyria with cerebellar dysplasia and Poretti-Boltshauser syndrome (associated to *LAMA1* alterations) (Poretti et al.

2016). Cerebellar dysplasia and cerebellar cysts can be observed also in combination with brainstem abnormalities and are described in the respective section (tubulinopathies, Joubert syndrome, Alpha-dystroglycanopathies).

## Cerebellar and brainstem malformations

### *Pontocerebellar hypoplasia*

Pontocerebellar hypoplasia (PCH) are a heterogeneous group of malformations characterized by the reduction in size of both pons and cerebellum. Besides the hypoplasia, the cerebellum can show also atrophy. To date, ten subtypes of PCH have been identified, defined by specific clinical and neuroradiological aspects and caused by recessive pathogenic variants in 14 different genes (Table 3).

**Table 3.** PCH subtypes with the causative genes, their respective chromosomal loci and the associated clinical features.

| PCH | Gene | Locus | Clinical features |
|---|---|---|---|
| PCH1 | EXOSC3<br>EXOSC8<br>VRK1<br>TSEN54<br>SLC25A46 | 9p13<br>13q13<br>14q32<br>17q25<br>5q22 | Axonal motor neuropathy |
| PCH2 | TSEN54<br>TSEN2<br>TSEN34<br>TSEN15 | 17q25<br>3p25<br>19q13<br>1q25 | Dyskinesias/chorea, “dragonfly” cerebellum |
| PCH3 | PCLO | 7q11-q21 | Optic atrophy, hearing impairment |
| PCH4 | TSEN54 | 17q25 | Abnormal-shaped bulbar olivary, myoclonus |
| PCH5 | TSEN54 | 17q25 | Abnormal-shaped bulbar olivary, myoclonus (letal in utero) |
| PCH6 | RARS2 | 6q15 | Reduced activity of mitochondrial respiratory chains, encephalopathies |
| PCH7 | TOE1 | 1p34 | Ambiguous genitalia (Vanishing testis) |
| PCH8 | CHMP1A | 16q24 | Reduced white matter, thin corpus callosum |
| PCH9 | AMPD2 | 1p13 | Cerebral cortex atrophy, corpus callosum abnormalities |
| PCH10 | CLP1 | 11q12 | Cerebral atrophy, thin corpus callosum, Spasticity/seizures, Absent or delay speech |

In some cases of PCH (PCH2 in particular), there is a greater involvement of the cerebellar hemispheres compared with the vermis

and this malformation assumes the aspect of a “dragonfly” on coronal neuroimages. When the hypoplasia of the cerebellar hemispheres is less severe, the malformation can be compared to a “butterfly” (Figure 2).

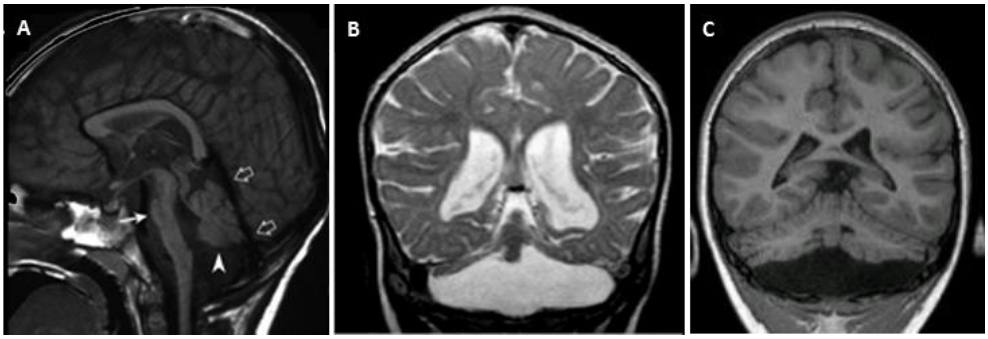


**Figure 2**. Midsagittal MR image showing hypoplasia of the pons and cerebellum (A); coronal images showing a cerebellar hypoplasia with more severe involvement of the cerebellar hemispheres with respect to the vermis (dragonfly appearance) (B) and a less severe hypoplasia of the cerebellar hemispheres (butterfly appearance) (C).

An X-linked dominant PCH is caused by loss of function variants in *CASK* and is characterized by a severe global cerebellar hypoplasia, pontine hypoplasia, microcephaly, severe cognitive impairment and deafness. Genetic alterations in *CASK* occur *de novo* and can be single nucleotide variants (SNVs) or copy number variants (CNVs). Other types of severe pontine and cerebellar hypoplasia may be accompanied by lissencephaly, a supratentorial morphologic anomaly

characterized by a lack of folds and grooves. This kind of malformation is caused mainly by recessive pathogenic variants in *RELN* and *VLDLR*, two genes of which *CASK* is a coactivator, that are involved in the regulation of neuronal migration pathway during the brain development. The cerebellar vermis is typically more affected than the hemispheres. Other peculiar signs are: lymphedema, seizures, microcephaly and cognitive impairment (Doherty et al. 2013).

### *Tubulinopathies*

A distinct class of malformations is caused mainly by *de novo* variants in genes involved in the formation and function of microtubules and is called “tubulinopathies”. The phenotypic spectrum associated with alterations in tubulin genes (*TUBA1A*, *TUBA8*, *TUBB2B*, *TUBB3* and *TUBB5*) is wide and includes severe intellectual disability, cerebral palsy, microcephaly, and seizures. Neuroimaging also shows a broad range of abnormalities: cerebellar dysplasia, cortical malformations (lissencephaly and polymicrogyria), dysmorphic basal ganglia, ventriculomegaly, corpus callosum anomalies and different degrees of pontocerebellar hypoplasia (Poretti et al. 2016).

### *Alpha-dystroglycanopathies*

Recessive pathogenic variants in genes (>15) responsible for the O-

glycosylation of alpha-dystroglycan are causative for a group of congenital muscular dystrophies affecting muscles, brain, and eyes. Phenotypes resulting from alterations in these genes are (in order of severity): Fukuyama disease, muscle-eye-brain disease, and Walker-Warburg syndrome. Neuroimaging findings are multiple and include infratentorial malformations (PCH, cerebellar dysplasia with cysts, pontomesencephalic kinking, ventral pontine cleft) and supratentorial anomalies (ventriculomegaly, polymicrogyria, hydrocephalus, cobblestone lissencephaly).

### *Joubert syndrome*

Joubert syndrome (JS) comprises a group of heterogeneous disorders that are uniquely characterized by a peculiar malformation of the brainstem and cerebellum called "molar tooth sign", characterized by cerebellar vermis hypodysplasia, thickening and malorientation of superior cerebellar peduncles and deepening of the interpeduncular fossa (Figure 3).

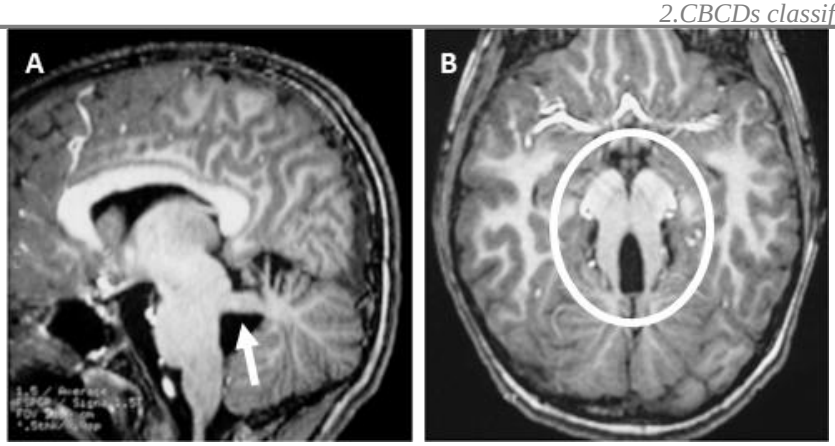


**Figure 3.** Midsagittal MR image showing elongated, thickened, and horizontally oriented superior cerebellar peduncles (A); axial MR image showing Deep interpeduncular fossa “Molar tooth sign” (B).

The typical neurological features of cerebellar impairment can remain isolated or may be accompanied with variable defects of other organs, among which: retina (Leber congenital amaurosis or progressive retinal dystrophy), kidneys (cystic disease or nephronophthisis), liver (congenital liver fibrosis) and skeleton (various types of polydactylies, ribs and other skeletal anomalies) (Romani et al. 2013) (Figure 4).

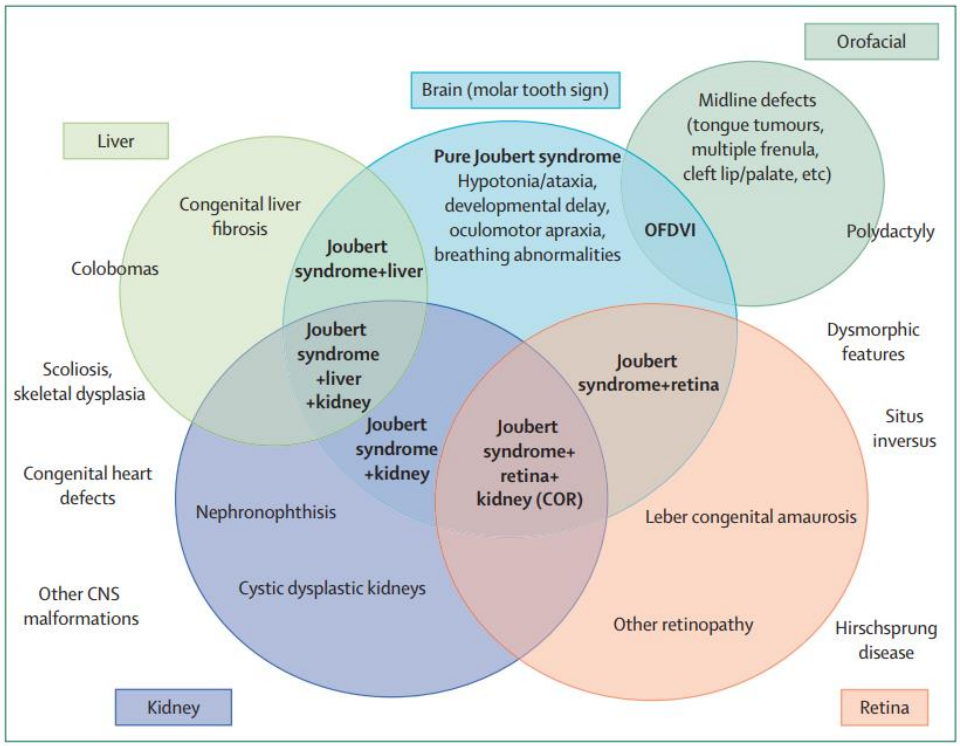


**Figure 4**. Multiorgan involvement in Joubert Syndrome (Romani et al. 2013).

Currently, up to 44 genes have been associated to JS (Table 4).

**Table 4.** Joubert genes and their respective chromosomal loci.

| ***Locus*** | ***Gene*** | ***Locus*** | ***Gene*** |
|---|---|---|---|
| 9q34 | INPP5E | 2q37 | PDE6D |
| 11q12 | TMEM216 | 1q42 | EXOC8 |
| 6q23 | AHI1 | 17q22 | MKS1 |
| 2q13 | NPHP1 | 17p11 | B9D1 |
| 12q21 | CEP290 | 19q13 | B9D2 |
| 8q22 | TMEM67 | 12q21 | POC1B |
| 16q12 | RPGRIP1L | 16p12 | KIAA0556 |
| 3q11 | ARL13B | 17p13 | TMEM107 |
| 4p15 | CC2D2A | 14q23 | KIAA0586 |
| Xp22 | OFD1 | 2p15 | TMEM17 |
| 2q24 | TTC21B | 1p36 | CEP104 |
| 15q26 | KIF7 | 1p36 | NPHP4 |
| 12q24 | TCTN1 | 5q23 | CEP120 |
| 12q24 | TCTN2 | 13q21 | PIBF1 |
| 2q33 | TMEM237 | 11q13 | C2CD3 |
| 7q32 | CEP41 | 17p13 | KIAA0753 |
| 11q12 | TMEM138 | 10q24.32 | SUFU |
| 5p13 | C5orf42 | 2q37.1 | ARMC9 |
| 10q24 | TCTN3 | 1p13.3 | CELSR2 |
| 16q12 | ZNF423 | 10q24.32 | ARL3 |
| 16q23 | TMEM231 | 4q28.1 | INTU |
| 8q13 | CSPP1 | 10q22.2 | FAM149B1 |

All these genes encode for proteins that play a role in the structure or functioning of the “primary cilium”, a subcellular organelle which dysfunction is responsible for a clinically and genetically overlapping

group of disorders called “ciliopathies” (Figure 5).

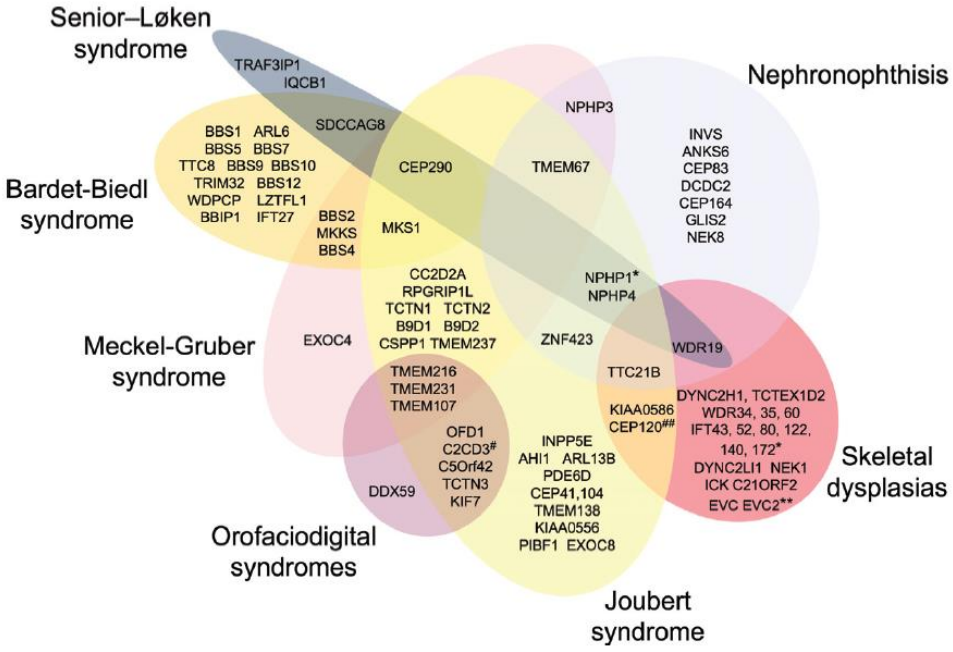


**Figure 5**. Genetic heterogeneity of primary ciliopathies and overlapping phenotypes (Mitchison et al. 2017).

### *Other rare CBCDs*

Another gene related to cerebellar and pontine malformations is *PTF1A*. Patients with recessive pathogenic variants in this gene present with facial dysmorphisms, neonatal diabetes mellitus and pancreatic insufficiency due to an agenesis of pancreas (Sellick et al.

2004). MRI shows agenesis/hypoplasia of the cerebellum. A recessive PCH-like phenotype can be caused by alterations in the *SEPSECS* gene. Pathogenic variants in this gene are responsible for progressive cerebellar and cerebral atrophy, spasticity, intellectual disability and, in some cases, seizures (Agamy et al. 2010). Progressive pontocerebellar hypoplasia is also typical in congenital disorders of glycosylation (type 1a), a recessive condition caused by pathogenic variants in *PMM2* gene (Matthijs et al. 1997). Patients have hypotonia and developmental delay but are also characterized by abnormal fat distribution, coagulopathy, retinal degeneration, peripheral neuropathy, stroke-like episodes and seizures.

## Predominantly brainstem malformations

### *Pontine Tegmental Cap Dysplasia*

The characteristic aspect of Pontine Tegmental Cap Dysplasia (PTCD) is represented by a vaulted pontine tegmentum (cap), flattened ventral pons and hypoplasia of the inferior and middle cerebellar peduncles. Other features include cranial nerves involvement (facial paralysis, trigeminal anesthesia, hearing loss, swallowing difficulty), congenital malformations (bone, kidney, heart). Prognosis is highly variable, and no genetic cause and familial recurrence have been yet reported.

### *Horizontal Gaze Palsy with Progressive Scoliosis*

A rare autosomal recessive condition is caused by *ROBO3* pathogenic variants and is called Horizontal Gaze Palsy with Progressive Scoliosis (HGPPS). This disorder consists in an absence of horizontal eye movements and a progressive development of scoliosis. MRI shows a butterfly-like medulla, prominent inferior olivary nuclei and hypoplastic pons.

### *Diencephalic-mesencephalic junction dysplasia*

This relatively recent malformation (Severino et al. 2016; Zaki et al. 2012) consists in a dysplasia of the diencephalic-mesencephalic junction and a midbrain with a peculiar butterfly-like aspect. Other

neuroradiological findings include corpus callosum agenesis/hypoplasia and ventriculomegaly. Clinical features are progressive microcephaly, spastic tetraparesis, severe cognitive impairment hypotonia and seizures. Very recently, two genes have been associated with diencephalic-mesencephalic junction anomalies (*PCDH12* and *FOXA2*) (Dines et al. 2019; Guemez-Gamboa et al. 2018).

# 3. Aims of the research

In the last few decades, especially after the spread of Next Generation Sequencing (NGS) techniques, it has been possible to identify several new genes causatives of CBCDs, including Joubert Syndrome (Romani et al. 2013) and Pontocerebellar Hypoplasia (Namavar et al. 2011). Nevertheless, pathogenic variants in known genes currently account for only about 60-70% of cases, suggesting the possibility of still uncovered causative genes. Moreover, despite a detailed classification of CBCDs, there is an important phenotypic overlapping between these disorders, as well as a genetic heterogeneity.

The aim of this PhD project is to better characterize the genetic basis underlying CBCDs and to improve genotype-phenotype correlations on a large number of patients. Another objective is to expand the current knowledge of CBCDs by looking for new genetic associations for diseases without a molecular diagnosis.

To reach these purposes a next-generation-sequencing (NGS) based approach has been adopted. Known causative genes have been screened by Custom Target Resequencing with specific gene panels and negative families then underwent Whole Exome Sequencing (WES) in order to identify novel causative genes. WES has been performed also in cases with peculiar brain malformations not attributable to any of the genes present in the panels.

# 4. Materials and methods

## Sample preparation

This PhD project has been carried out on a large cohort of CBCD patients recruited through national and international collaborations. In order to achieve a diagnosis as precise as possible, each patient has been carefully characterized through a detailed clinical questionnaire and an accurate review of brain neuroimaging from expert pediatric neuroradiologists. To participate in this study, parents or legal representatives signed an informed consent concerning the use of data and biological material for research purposes. Blood or DNA samples have been obtained from probands, parents, affected and unaffected siblings, when available.

In the case of blood samples, genomic DNA has been isolated using spin column kit (NucleoSpin Blood, Macherey-Nagel). DNA integrity has been assessed through gel electrophoresis on a 0.8% agarose gel and confirmed by the visualization of a fragment around 23.1 kb without a smear, which is a sign of sample degradation. Sample quality has been verified by a spectrophotometric analysis (NanoDrop 1000, Thermofisher), considering acceptable quality values (260/280 and 260/230) between 1.80 and 2.20. The exact quantity has been estimated with a fluorometric assay (Qubit, Invitrogen) which involves the use of an intercalating fluorescent dye specific for double stranded DNA (dsDNA) in order to avoid estimating errors due to contaminants

quantification.

RNA samples for functional characterization of identified variants have been isolated from whole blood or fibroblasts with Total RNA Mini Kit (Geneaid) and converted in cDNA by reverse trascription (RT) with PrimeScript RT-PCR Kit (Takara). RT reaction has been prepared as follow: 2µl of 5X PrimeScriptTM Buffer, 0.5µl of 1X PrimeScriptTM RT Enzyme Mix I, 0.5µl of Oligo dT Primer (50µM), 0.5 µl of 25 pmol Random 6 mers (100 µM), 50 pmol total RNA and RNase Free $dH_2O$ to a final volume of 10µl. Thermocycler has been set up with 15' at 37°C for reverse transcription and 5'' at 85°C for reverse transcriptase inactivation.

## Next Generation Sequencing

In this project, a combined NGS based approach has been used:

- Custom Target Resequencing for screening of known causative genes selected through specific probes specified during the gene panel design with SureDesign tool (Agilent Technologies). Two different gene panels have been used: the first containing probes for 54 genes associated with Joubert Syndrome (Supplementary Table 1) and the second specific for 41 genes causative for the other CBCDs (Supplementary Table 2)

- Whole Exome Sequencing for probands and relatives who were

negative to the known gene screening. This approach allows sequencing the whole coding portion of the genome.

These approaches require a similar upstream preparation of DNA libraries which has been performed through a Hybridization and Capture technology (SureSelect XT/QXT, Agilent Technologies). Libraries have been sequenced on an Illumina MiSeq sequencer in the case of gene panels whereas an Illumina HiSeq 2500 instrument has been used for WES.
In particular, the library preparation protocol used includes the following steps:

- Genomic DNA fragmentation, which can be enzymatic or mechanical, the latter with a Covaris sonicator that requires additional steps for the ends repair and the 3' end adenylation, interspersed with magnetic beads purifications.
- Ligation of adaptor sequences, needed for sequencing reaction (in the enzymatic fragmentation, this step is performed in a single reaction).
- Purification with magnetic beads, amplification of the adaptor-tagged libraries and clean-up.
- Quantity and quality assessment of DNA library through capillary electrophoresis (TapeStation and Bioanalyzer, Agilent).
- Hybridization with a Capture Library containing the biotin

labeled probemix specific for the genomic region to analyze.

- Capture of the targeted molecules with streptavidin beads (by biotin-streptavidin interaction).
- Amplification of the captured library with the addition of an index sequence unique for each sample and purification with magnetic beads.
- Quantity and quality assessment of DNA library.
- Pooling of samples for multiplexed sequencing.

The sequencing reaction occurs on a flow cell within the sequencer. The flow cell is a glass slide containing small fluidic channels, through which polymerases, dNTPs and buffers can be pumped. The glass inside the channels is coated with short oligonucleotides complementary to the adapter sequences. The DNA library containing adapters is diluted and hybridized to these oligonucleotides. Library strands are amplified using a "bridge-PCR" strategy employing cycles of primer extension followed by chemical denaturation. At the end of amplification, small clusters of identical DNA molecules immobilized on the surface are sequenced *en masse*.

## Bioinformatic analysis

Bioinformatic analysis was carried out aligning raw sequences data to the human reference genome (GRCh37) using BWA v0.7.5 as a first step. Variants were called with GATK Unified Genotyper, annotated

through the eVANT v1.3 software (enGenome). The resulting variants have been filtered for minor allele frequency (MAF) in the general population (considering rare a variant with MAF<1%), functional consequence (nonsynonymous, exonic and splicing variants) and inheritance model (X-linked, recessive and *de novo* models).

As WES aims at identifying new genetic associations, an additional step for variant interpretation is required. During this step, different aspects have been considered through the consultation of different bioinformatic tools and databases. For instance, the physical-chemical consequence of an amino acid change was evaluated with *in silico* prediction tools of pathogenicity (SIFT, PolyPhen, CADD, etc.), which can suggest if the amino acid change could be tolerated or deleterious for the protein structure and functionality. Another aspect considered through bioinformatics tools is the phylogenetic conservation of the variant position across species (GERP, PhyloP): a variant located in a highly conserved position is more probable to have a deleterious effect compared to a variation in a non-conserved region. If a variant is known, it has an identification code and can be found in online databases (dbSNP, ClinVar, HGMD, Varsome) which may indicate if the variant is associated with a disease and classified as benign or pathogenic. Moreover, the minor allele frequency in the general population has been evaluated using online databases (1000G, EVS, GnomAD, the latter may also indicate the tolerance of a gene to variations). Finally, important aspects considered are also the tissue expression of the gene, the interacting protein network and the

molecular pathway involved (GeneCards, GTEx). *In silico* prediction of a potential alteration of splicing has been evaluated with Human Splicing Finder v3.1, while alteration of amino acid reading frame has been assessed through Expasy (Swiss Institute of Bioinformatics). Relevant variants have been confirmed by Sanger sequencing on probands and segregation analysis has been performed on both parents.

## Sanger sequencing

Genomic DNA and cDNA samples have been amplified by Polymerase Chain Reaction (PCR) with specific primer pairs designed with Primer3 tool. Primer specificity has been assessed through Primer BLAST tool. PCR reaction has been carried out with 1U of GoTaq (Promega) polymerase, 1X Buffer (with $MgCl_2$), 0.2 mM dNTPs, 1µM Forward and Reverse Primer, 50ng of genomic DNA and $dH_2O$ to a final volume of 25 µl. Thermocycler has been set up with an initial denaturation at 94°C for 5' followed by 35 cycles of: 30'' at 94°C, 30'' of primer annealing (variable temperature depending on primer sequence) for 30'' and 30'' at 72°C, with a final extension at 72°C for 7'. PCR products have been controlled on a 1.8% agarose gel and subjected to enzymatic purification with ExoSap (Affymetrix) in incubation at 37°C for 30' (enzyme activation) followed by 30' at 80°C (enzyme deactivation). Multiple PCR products have been separated by gel excision and purified through Zymoclean Gel DNA Recovery kit

(Zymo Research). Sequencing reaction has been performed with 1µl of BigDye Terminator v3.1 (Applied Biosystems), 1X Buffer, 1µM Primer Forward or Reverse (in two different reactions) and $dH_2O$ to a final volume of 10µl. Thermocycler program used was: 98°C for 5' and 30 cycle of 96°C for 10'', 56°C for 5'' and 60°C for 4'. Sequences have been purified with DyeEx 2.0 Spin Kit (Qiagen) and ran on a 3130xl Genetic Analyzer (Applied Biosystems). Sequence analysis has been performed with MutationSurveyor (Softgenetics) software.

## Multiplex Ligation-dependent Probe Assay

Copy number variations in the *CASK* gene have been analyzed by Multiplex Ligation-dependent Probe Assay (MLPA) with the SALSA MLPA Probemix P398 (MRC-Holland). In particular, 100ng of genomic DNA have been denatured in a thermocycler at 98°C for 5'and cooled to 25°C. Then, a hybridization master mix (containing 1.5µl of MLPA Buffer and 1.5µl of probemix for each sample) was added, and the sample was denatured at 95°C for 1' and hybridized at 60°C for 16-20 hours. Subsequently, a ligation reaction has been performed by adding 25µl of $H_2O$, 3µl of Buffer A and Buffer B and 1µl of Ligase65 enzyme for each sample and incubating the reaction for 15' at 54°C, followed by 5' at 98°C for enzyme inactivation. The final step consists in a PCR reaction with: 7.5µl of $dH_2O$, 2µl of SALSA PCR primer mix and 0.5µl of SALSA polymerase. Thermocycler program comprises 35 cycles of: 95°C for 30'', 60°C for 30'', 72°C for 60'' and a final extension

of 72°C for 20'. Amplified fragments have been separated by capillary electrophoresis on a 3130xl Genetic Analyzer (Applied Biosystems) and analyzed with Coffalyser.Net Software (MRC-Holland). After intrasample and intersample normalization of data, it is possible to detect genomic duplications and deletions based on the peak height and with a Dosage Quotient (DQ) value. DQ values between 0.80 and 1.20 are indicative for a normal dosage. DQ values <0.65 represent a genomic deletion while DQ values >1.30 a duplication. Each identified CNV has been validated by Real time PCR.

## Real time PCR

Real time PCR (RT-PCR) has been performed on 10ng of genomic DNA with 12.5µl of SYBR Green PCR Master Mix (Applied Biosystems) and 0.5µl of Primer mix (containing 10µM of each primer) for each sample. Sample normalization has been performed with Telomerase (*TERT* as housekeeping gene) and using two control samples, considering an average of three concentration values for each sample (in triplicate). Each RT-PCR reaction has been performed on a 7900HT Real-Time PCR System (Applied Biosystems) with the following program (standard modality): 2' at 50°C, 95°C for 10', 40 cycles of 15'' at 95°C and 1' at 60°C followed by a dissociation curve to assess primer specificity.

# 5. Results

## Custom Target Resequencing

### *Joubert syndrome*

During this PhD project I contributed to expand an existing cohort of Joubert syndrome families with 298 newly recruited patients, bringing the overall cohort to a total of 444 JS families. Pathogenic variants have been identified in a total of 264 (59%) probands (Supplementary table 3). Most frequently mutated genes were: *C5orf42* (8%), *CEP290* (7%), *CC2D2A* (7%), *AHI1* (7%), *TMEM67* (5%) (Figure 6).

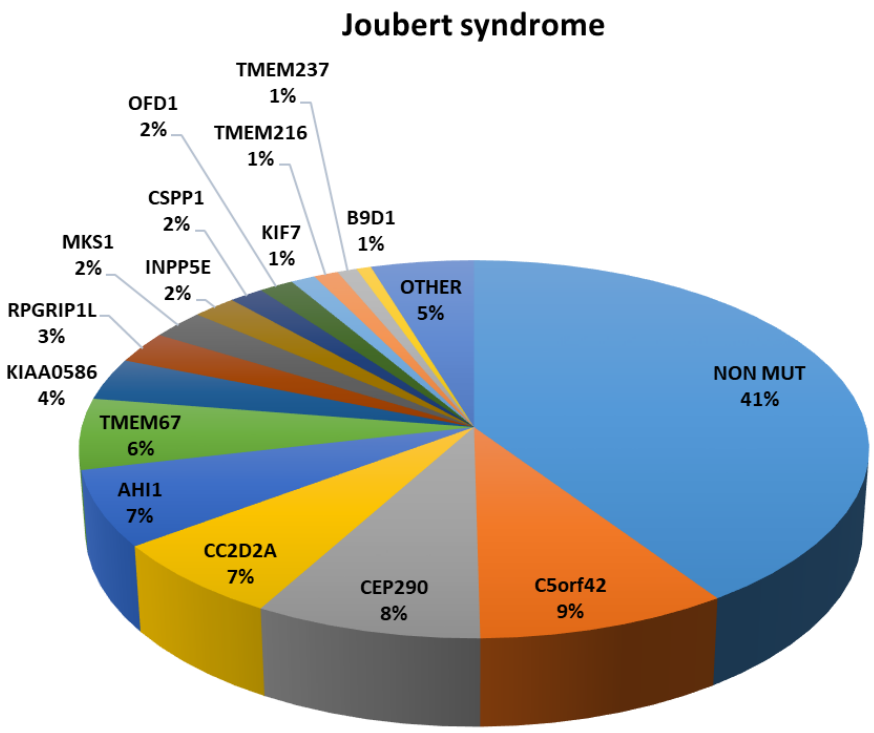


**Figure 6**. Frequency of pathogenic variants in known Joubert Syndrome genes.

### *Pontocerebellar hypoplasia*

During the project, 64 newly recruited PCH probands underwent Custom Target Resequencing. Pathogenic variants have been

identified in 43 (67%) of them (Supplementary table 4). The most commonly mutated genes were: *CASK* (35%, 23/64), *TSEN54* (16%, 10/64), *EXOSC3* (5%, 3/64), *RARS2* (1.75%, 1/64), *VLDLR* (1.75%, 1/64), *TOE1* (1.75%, 1/64), *PMM2/ATP2B3* (1.75%, 1/64). Notably, *CASK* variants include 15 single nucleotide variants and 8 CNVs identified by MLPA analysis, while 33 PCH probands were negative to deletion and duplication analysis (Figure 7).

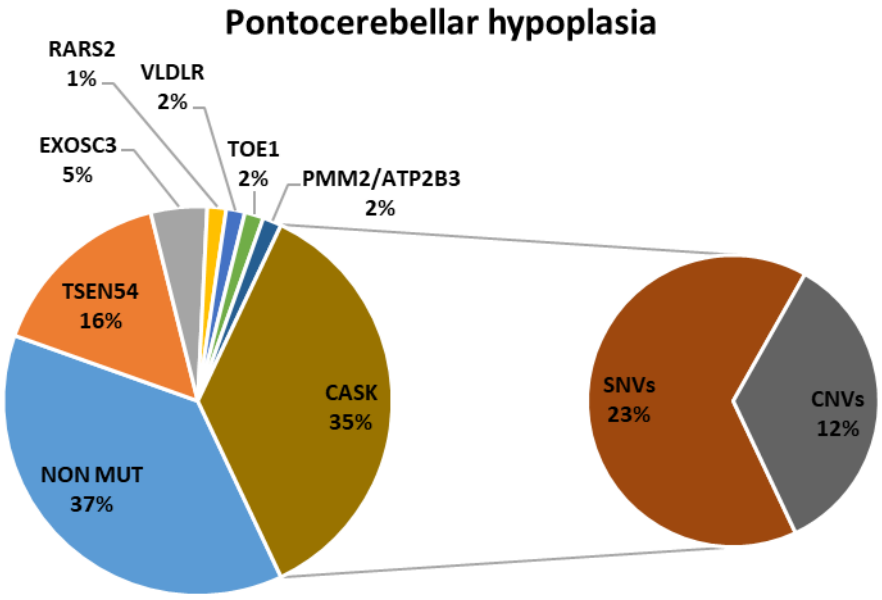


**Figure 7**. Frequency of pathogenic variants in Pontocerebellar Hypoplasia genes.

### *Other CBCDs*

Concerning other CBCDs, pathogenic variant frequency in the phenotypic subgroups is as follows: HGPPS 100% (2/2); PBS 93% (14/15); WCH 33% (2/6); NPCA 7% (2/28); other CBCDs 17% (2/12). (Figure 8, Supplementary table 5)

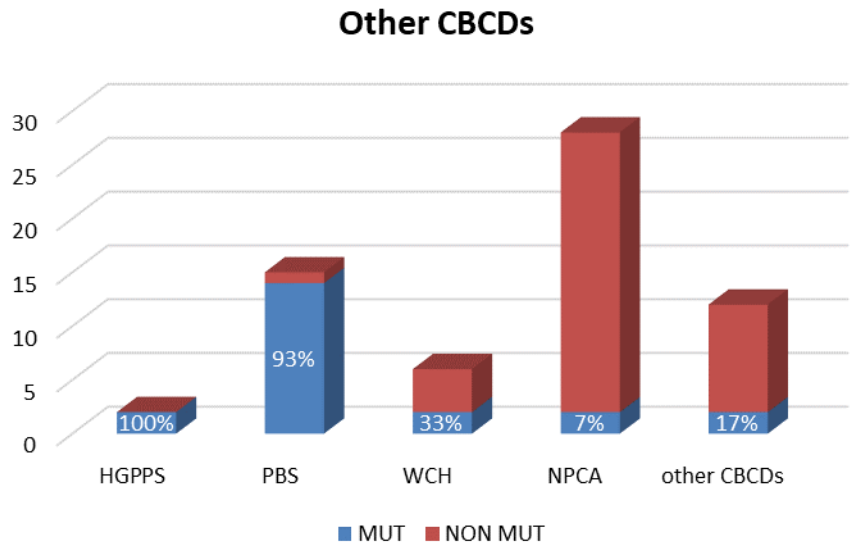


**Figure 8.** Percentage of pathogenic variants identified in other CBCDs.

### *SPTBN2*

A heterozygous missense variant (c.1438C>T, p.Arg480Trp) in the *SPTBN2* gene has been identified in a 2-year-old girl presenting with a congenital severe form of cerebellar ataxia. Brain MRI showed global cerebellar hypoplasia with enlarged interfolial spaces. Segregation

analysis revealed the *de novo* occurrence of this variant as it was not identified in the parents (Figure 9). Usually, heterozygous *SPTBN2* variants cause an adult-onset Spinocerebellar Ataxia, while homozygous variants are associated with a recessive form of Spinocerebellar ataxia with early onset.

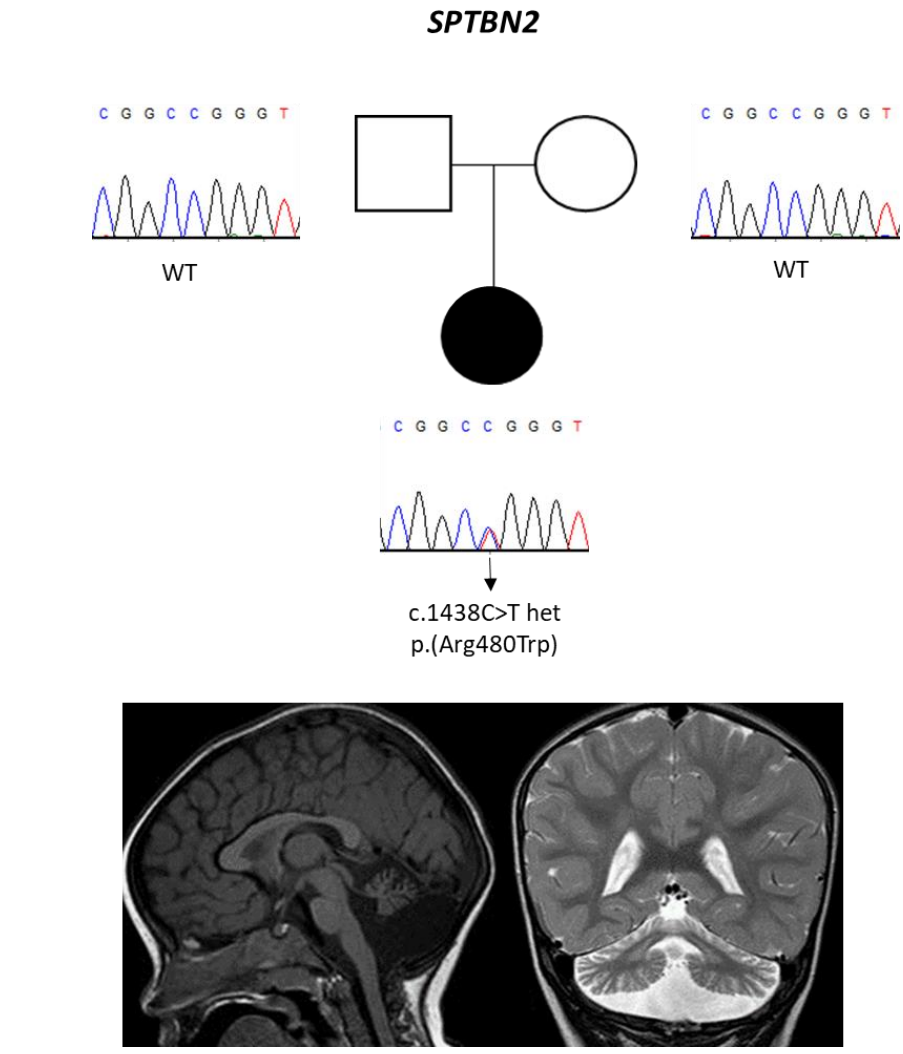


**Figure 9.** Segregation analysis of *SPTBN2* variant (on the top) and MR images showing the global cerebellar hypoplasia of the proband (at the bottom).

## Whole Exome Sequencing

During the three PhD years, a total of 39 negative CBCD families and cases with other peculiar brain malformations, underwent Whole Exome Sequencing in order to identify new candidate genes.

### *SUFU*

The first candidate gene identified (*SUFU*) was found mutated in two siblings, born from consanguineous parents and presenting with mild Joubert Syndrome, polydactyly and peculiar dysmorphic features (broad forehead, hypertelorism, macrocephaly, deep nasal bridge). MRI showed mild “Molar Tooth” sign, mild vermis hypoplasia and asymmetric perisylvian polymicrogyria. The identified variant is a homozygous missense variant (c.1217T>C, p.Ile406Thr) inherited from both parents that are heterozygous carriers (Figure 10).

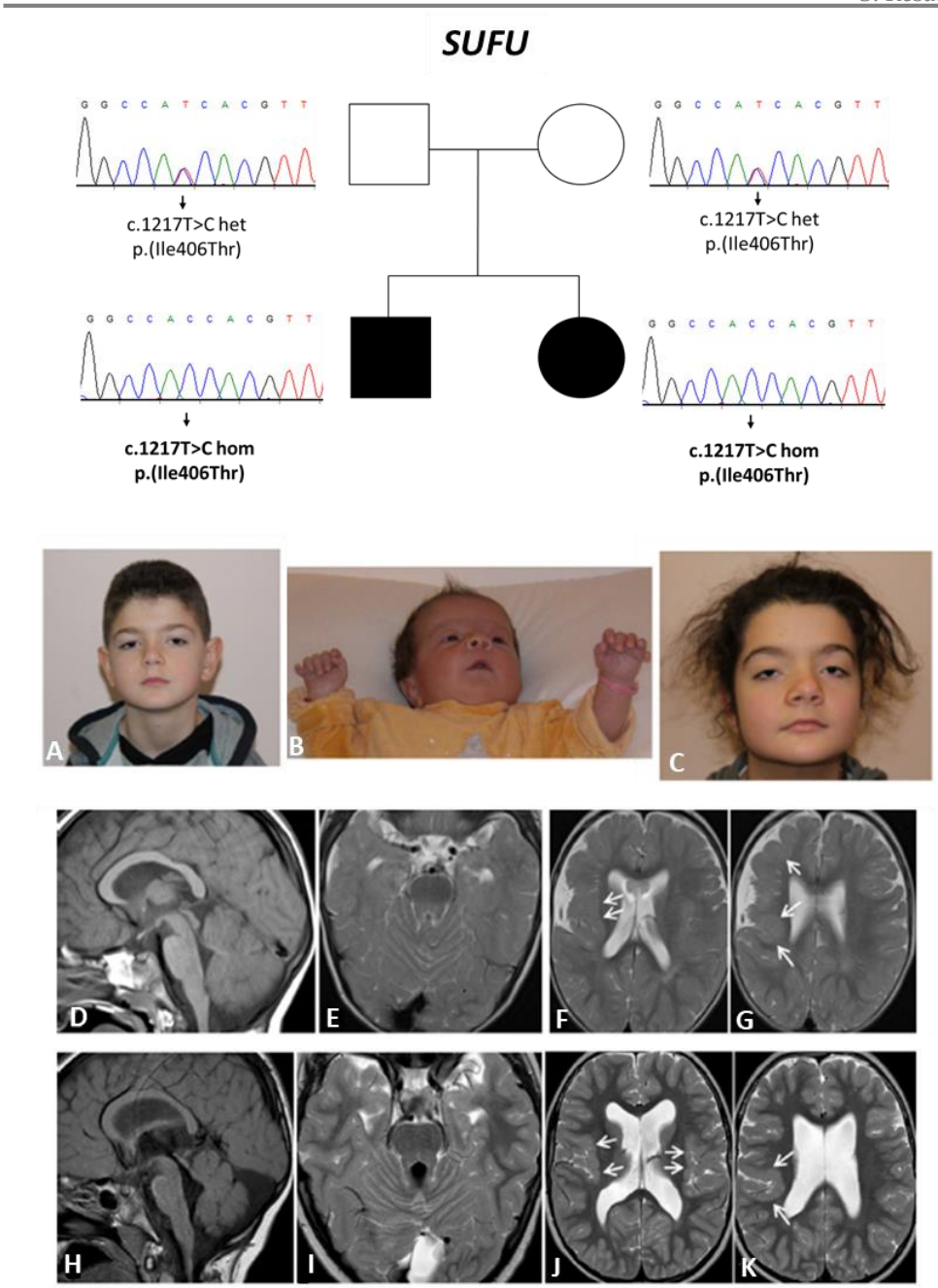


**Figure 10**. From the top: segregation analysis of *SUFU* variant; pictures of

the affected siblings showing dysmorphic facial features (A, C) and polydactyly (B); MR images showing mild vermis hypoplasia (D, H), mild "molar tooth" sign (E-I), bilateral polymicrogyria (F, G, J, K).

This variant was absent in GnomAD and predicted to be deleterious by most of the *in silico* prediction tools (SIFT, PolyPhen, Mutation Taster, Mutation Assessor, DANN, CADD).

I performed Sanger validation and segregation analysis as well as a genetic screening of the 12 exons of *SUFU* in a cohort of 60 patients with familial polymicrogyria and in 100 Italian controls. This further screening failed to identify any pathogenic variant in these two cohorts.

### *GSX2*

Pathogenic recessive variants in the second gene (*GSX2*) were identified in two sporadic unrelated children with a severe neurological phenotype (severe intellectual impairment, spasticity, involuntary movements), who shared a highly peculiar brain malformation, characterized by hypothalamic-mesencephalic fusion, absence of putamina and of globi pallidi and hypoplasia of the olfactory bulbs. The missense variant c.752A>G p.(Gln251Arg) has been identified in a child born from nonconsanguineous parents, while the proband with the nonsense variant c.26C>A p.(Ser9*) had consanguineous parents (Figure 11). All *in silico* prediction tools reported the deleteriousness of the missense variant as well as most of the applicable tool for the nonsense variant (DANN, Mutation Taster, CADD). Moreover, both

variants were absent in GnomAD.

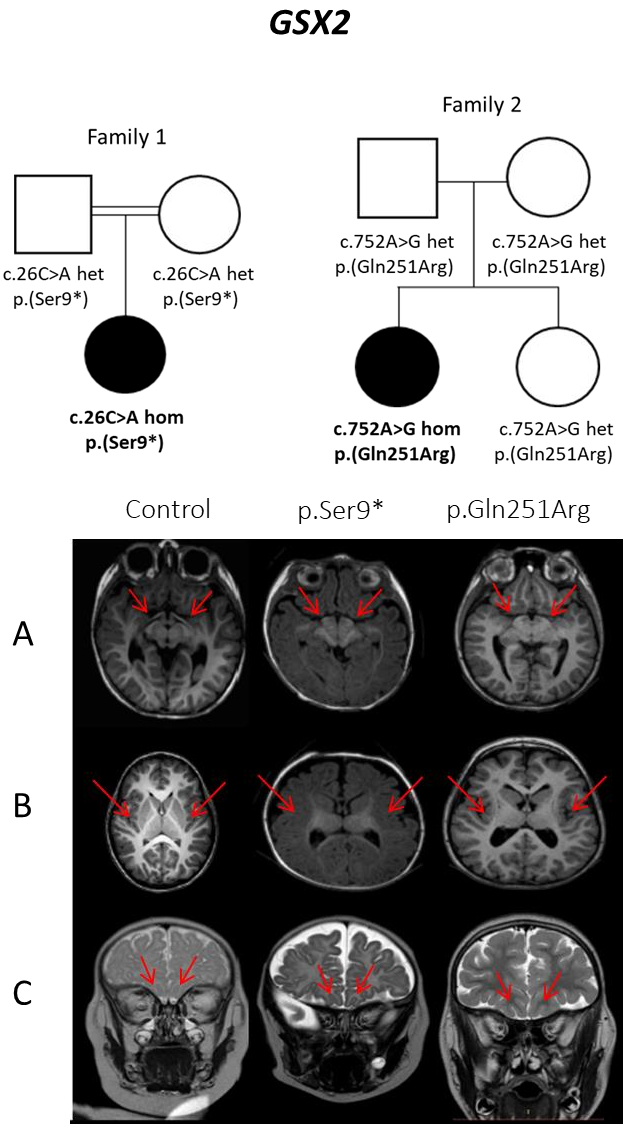


**Figure 11**. From the top: segregation analysis of the *GSX2* nonsense

variants p.(Ser9*) in Family 1 and the missense variant p.(Gln251Arg) in Family 2; MR images of the patients versus a control showing hypothalamus-mesencephalic fusion (A), absence of putamina (B) and olfactory bulbs hypoplasia (C).

In this project, my contribution was to confirm the identified variant in this family by Sanger sequencing and to sequence *GSX2* in a group of 10 patients with abnormalities of the mesencephalic-diencephalic junction. Moreover, I validated site-directed mutagenesis of *GSX2* cloned in an expression vector for subsequent functional studies.

### *TTL*

I performed library preparation for WES, data analysis and Sanger validation in two sisters, born from consanguineous parents, presenting with generalized hypotonia and global developmental delay. MRI showed hypoplasia of the cerebellar vermis and corpus callosum, enlarged cisterna magna, brainstem dysplasia and dysmorphic basal ganglia.

After bioinformatic analysis, the best candidate which survived filtering was a homozygous missense variant (c.1013G>A, p.Cys338Tyr) in the *TTL* gene (Figure 12). Most of the *in silico* tools predicted a deleterious effect of this amino acid change (SIFT, PolyPhen, Mutation Taster, Mutation Assessor, CADD) and the variant was not reported in GnomAD.

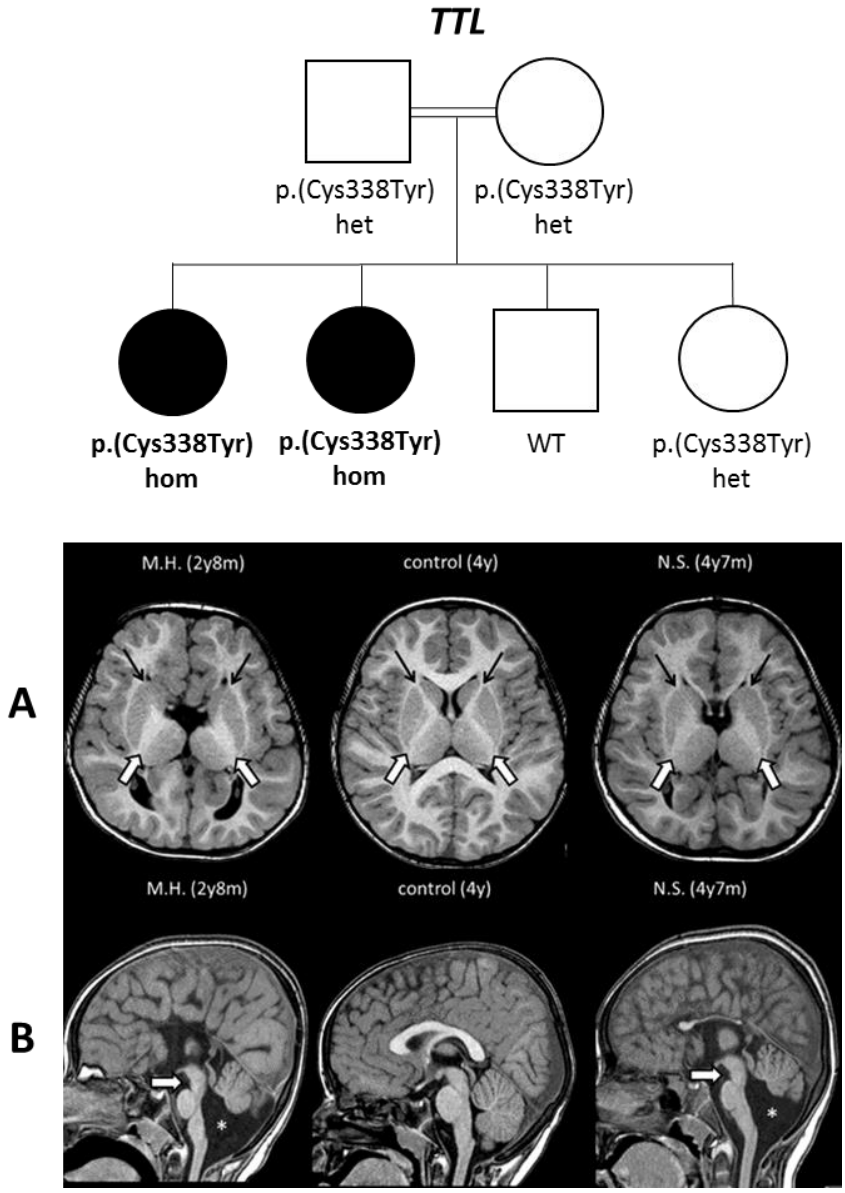


**Figure 12**. From the top: segregation analysis of the *TTL* variant; MR images of the two affected siblings versus a control showing Dysmorphic basal ganglia (upper black and white arrows) (A); hypoplasia of the cerebellar vermis and corpus callosum, enlarged cisterna magna (*), brainstem dysplasia (lower white arrows) (B);

### *IRF2BPL*

Whole Exome Sequencing has been performed in an 8-years old girl, without consanguinity in family, presenting with a neurodegenerative clinical picture characterized by the presence of a progressive hypopostural tetraparesis, dysarthria and intellectual disability. Brain MRI showed slight increase in the size of the ventricular system and skin biopsy revealed the presence of osmiophilic lysosomal deposits. WES analysis demonstrated a heterozygous deletion of seven base pairs resulting in a frameshift and insertion of a premature stop codon after 13 amino acids (c.490_496delGCGGTGG, p.Ala164Asnfs*13) in the *IRF2BPL* gene. This variant was absent in both parents suggesting a *de novo* occurrence (Figure 13). GnomAD showed the presence of several inframe variants in the region containing the deletion but no frameshift variants were reported.

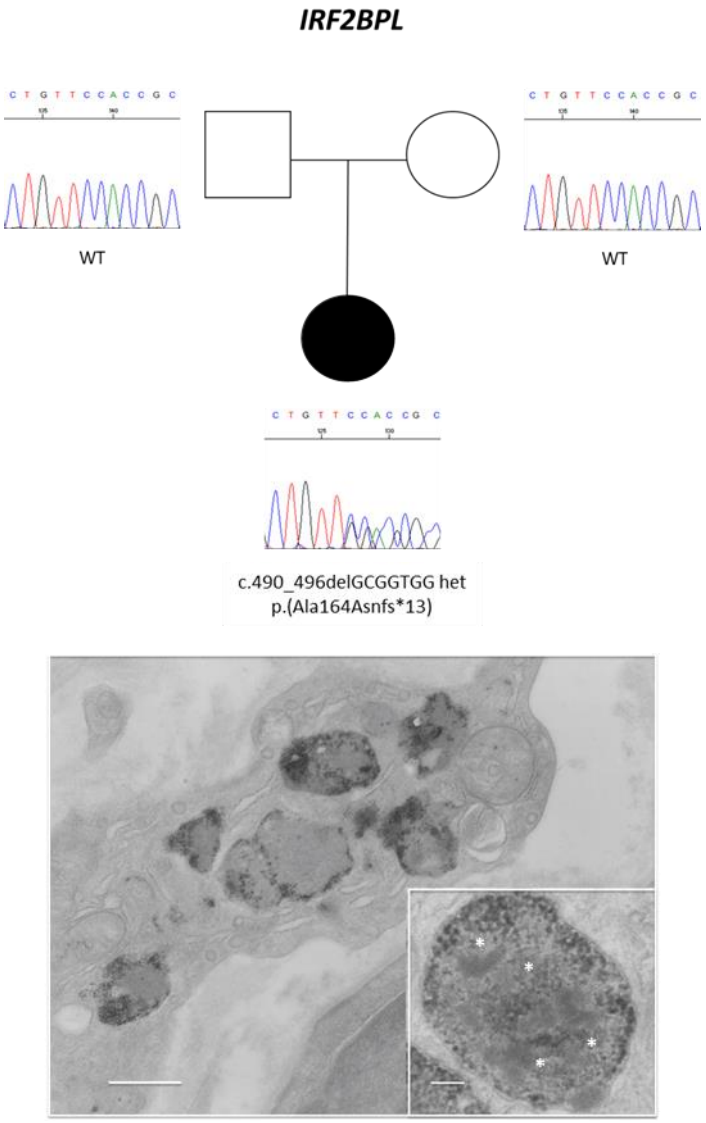


**Figure 13**. At the top: segregation analysis of the *IRF2BPL* variant; At the bottom: Electron microscopy image of the skin biopsy showing enlarged lysosomes storing osmiophilic material. Insert: a lysosome filled with granular material and scattered curved tubular aggregates (*). bar=1µm (figure); =0.15µm (insert).

### *KIF1A*

Another pathogenic variant identified through WES was found in a boy, born from a non-consanguineous family, showing a severe clinical picture of hypotonia, spastic tetraparesis, seizures and nystagmus. MRI showed cerebellar atrophy, thinning of optic chiasma and hyperintensity of posterior white matter and of dentate nuclei. The presence of axonal spheroids in peripheral nervous system suggested the diagnosis of Infantile Neuroaxonal Dystrophy (INAD). WES analysis demonstrated the presence of a *de novo* heterozygous missense variant (c.920G>A, p.Arg307Gln) in the *KIF1A* gene (Figure 14).

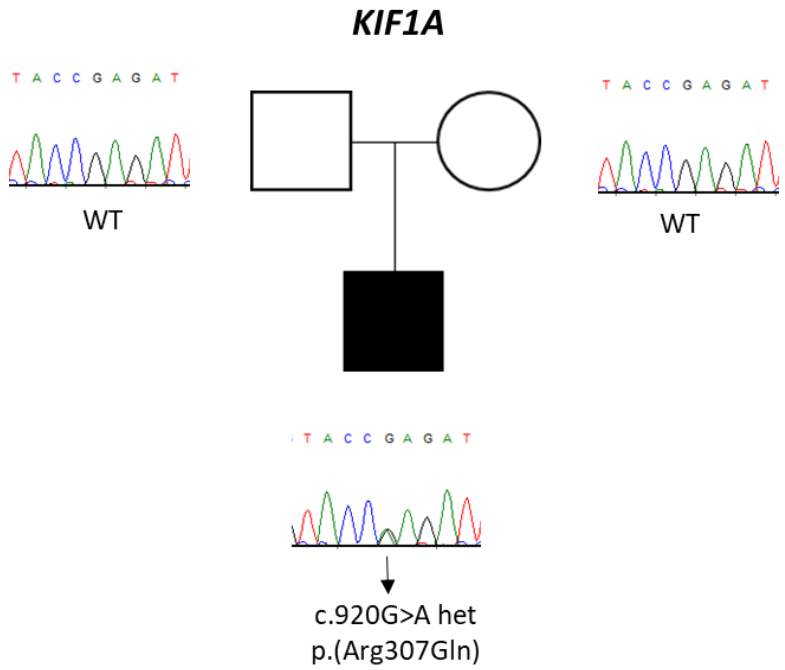


**Figure 14**. Segregation analysis of the *KIF1A* variant

### *BRAT1*

WES analysis was performed in two brothers presented with nonprogressive congenital ataxia and mild intellectual impairment. Brain imaging demonstrated a cerebellar atrophy of moderate degree, which however did not progress over time, as established by consecutive MRI scans performed at age of 18 months and 6 years.

Segregation analysis confirmed the presence of two compound heterozygous pathogenic variants in the *BRAT1* gene: c.638dupA p.(Val214Glyfs*189) and c.1395G>A p.(Thr465Thr) (Figure 15).

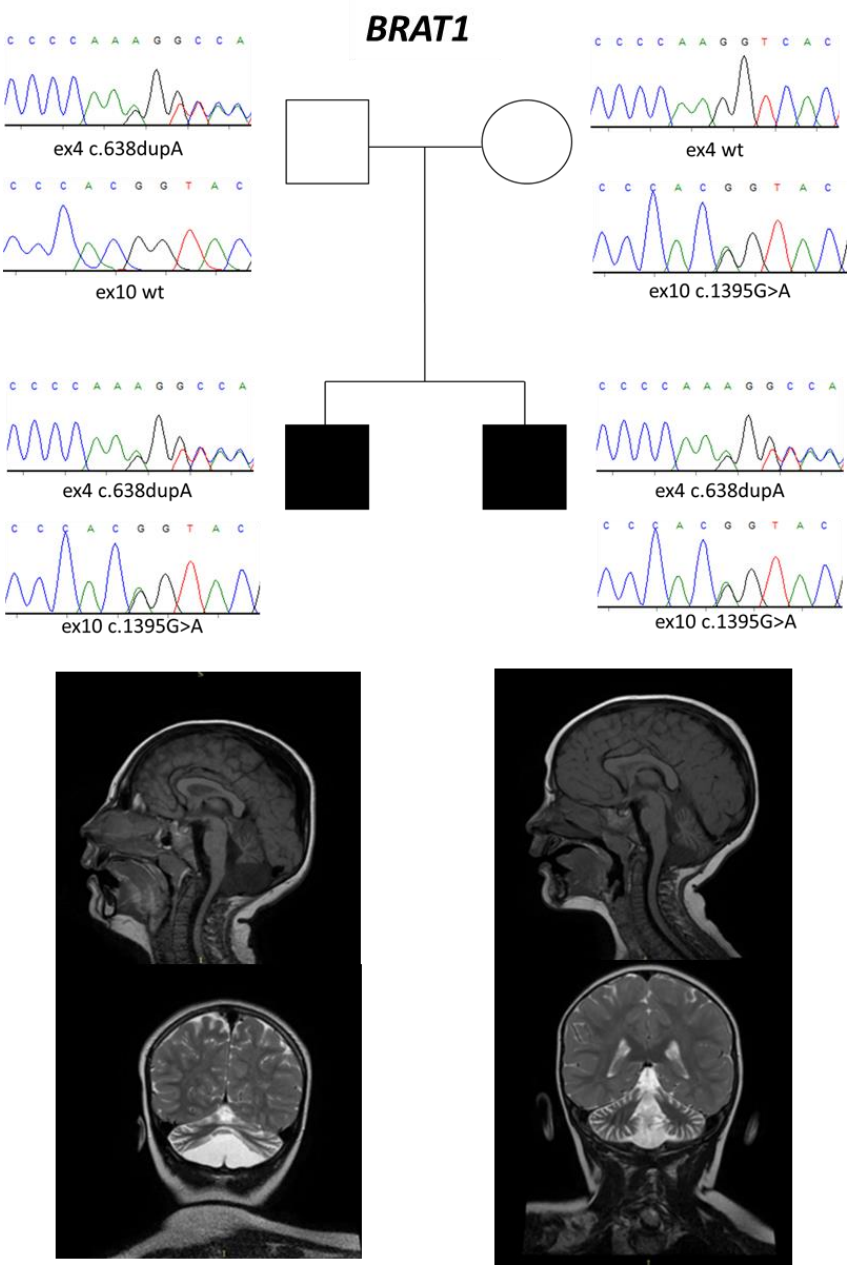


**Figure 15**. From the top: segregation analysis of the *BRAT1* variant; midsagittal and coronal MR images of the two brothers showing the cerebellar atrophy

The c.638dupA variant was known to be pathogenic and is predicted to alter the reading frame until a premature stop codon after 189 amino acid (p.Val214Glyfs*189). The synonymous variant c.1395G>A p.(Thr465Thr) was novel and predicted (by Human Splicing Finder) to alter the splicing process as it involves the last nucleotide of exon 10. I investigated this potential alteration by sequencing the region containing the flanking exons (9-11) on cDNA samples obtained from whole blood of affected siblings and healthy parents. I observed an exclusion of exon 10 and the consequent fusion between exon 9 and exon 11 (Figure 16).

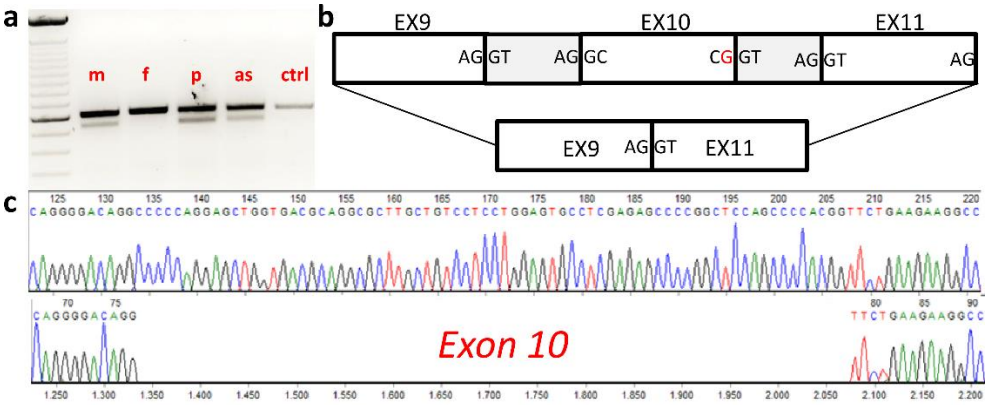


**Figure 16**. Functional characterization of *BRAT1* synonymous variant. Gel image of cDNA amplification showing two bands of different weight: the bigger is the WT product, the smaller is the mutated with 74bp of difference (a); schematic representation of the fusion between exon 9 and exon 11 (b); electropherogram showing the lack of exon 10 in the mutated sequence (at the bottom) compared with a reference sequence (at the top) (c).
m, mother; f, father; p, proband; as, affected sibling; ctrl, control.

Since exon 10 is characterized by 74 bp (not multiple of 3), the reading

frame resulting from the fusion between exon 9 and 11 is altered and it leads to a premature stop codon after 23 amino acids. Given these observations the resulting variant is c.1323_1396del; p.(Pro442Serfs*23).

### *FSD1L*

I performed a detailed molecular characterization of the homozygous missense variant (c.409T>G, p.Leu137Val) in *FSD1L* previously identified through WES in two siblings presenting with neurodevelopmental delay, intellectual disability, seizures, optic atrophy and spastic tetraparesis. Neuroimaging showed thin corpus callosum, mild ventricular dilatation, reduced white matter, mild hyperintensity of posterior periventricular white matter (Figure 17).

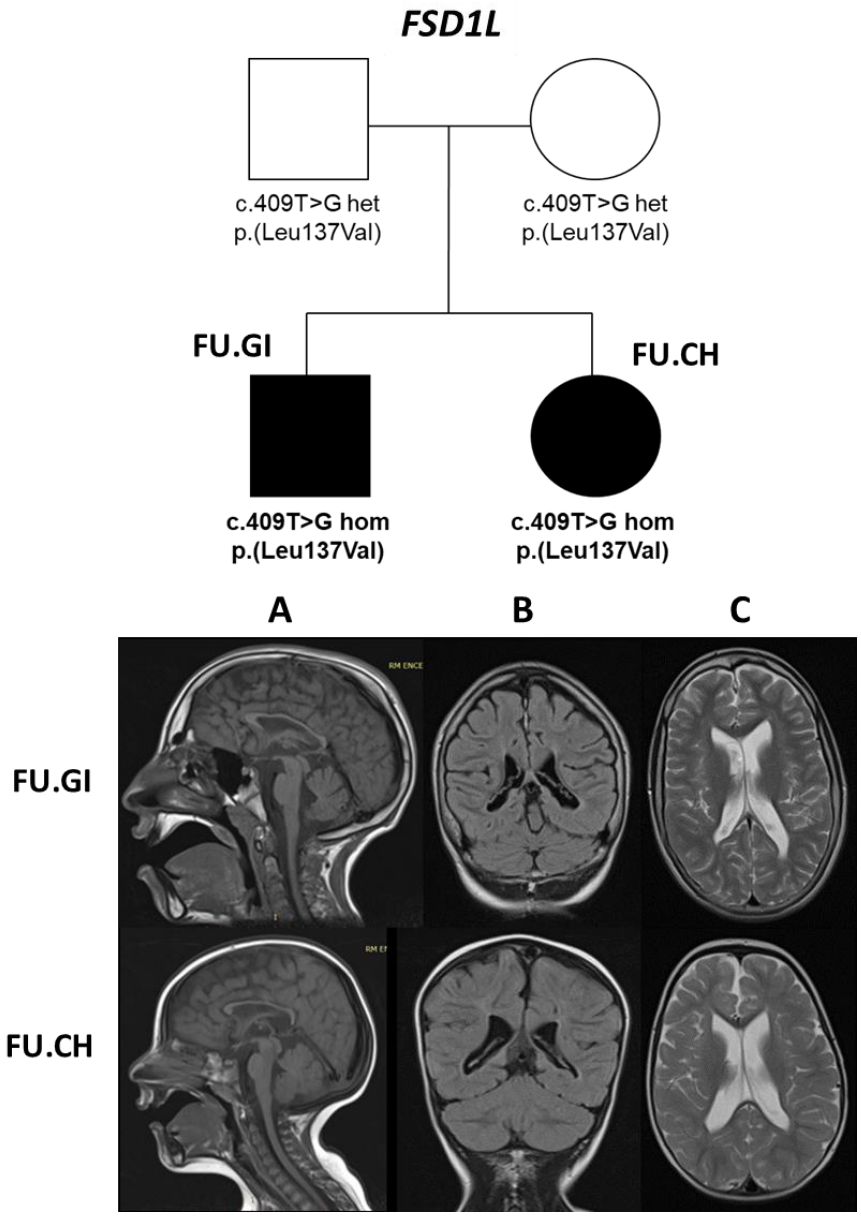


**Figure 17**. From the top: segregation analysis of *FSD1L* variant. MR images of the two siblings showing thin corpus callosum (A), mild ventricular dilatation and reduced white matter (B), mild hyperintensity of posterior periventricular white matter (C).

In particular, I have amplified and sequenced the region containing the missense variant on patients' cDNA samples from fibroblasts and I found that this variant creates a cryptic exonic splicing site leading to a premature truncation of the exon containing the variant (4 nucleotides upstream the variation), the exclusion of the subsequent exon and the fusion with the second exon after. Posterior prediction analysis with Human Splicing Finder confirmed the possible activation of a cryptic splicing site, while only SIFT (with low confidence) revealed a deleterious effect of the genomic nucleotide change. The deletion in *FSD1L* was predicted (by ExPASy) to cause the lack of 20 amino acids, conserving the downstream reading frame. Interestingly, cDNA samples from control fibroblasts showed two different transcript isoforms, the first lacking one exon (exon 5), the second lacking two exons (exon 5 and 6). A cDNA sample obtained from a total brain RNA extract showed a full-length *FSD1L* isoform (containing exon 4, 5 and 6) (Figure 18).

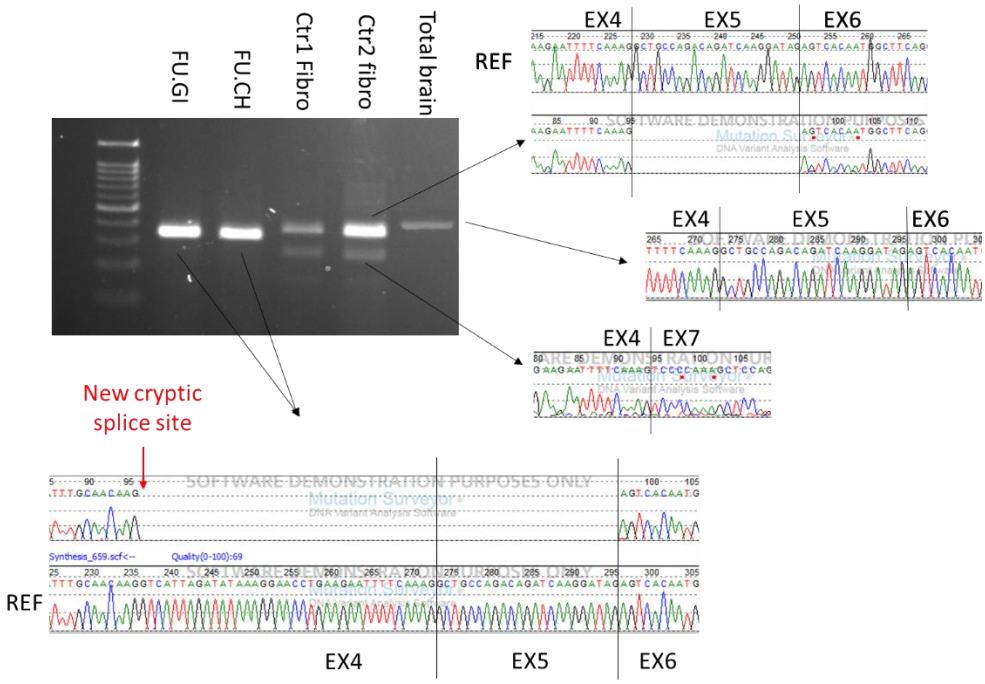


**Figure 18**. Analysis of the *FSD1L* variant on cDNA from patients and from two fibroblasts' controls and a total brain control. Gel image shows the products of cDNA amplification. Electropherograms show the sequences of the different isoforms obtained.

Given these evidences, I designed a series of primer pairs in order to isolate the eight isoforms of *FSD1L* (Figure 19) and to investigate the expression of each isoform in different tissues.

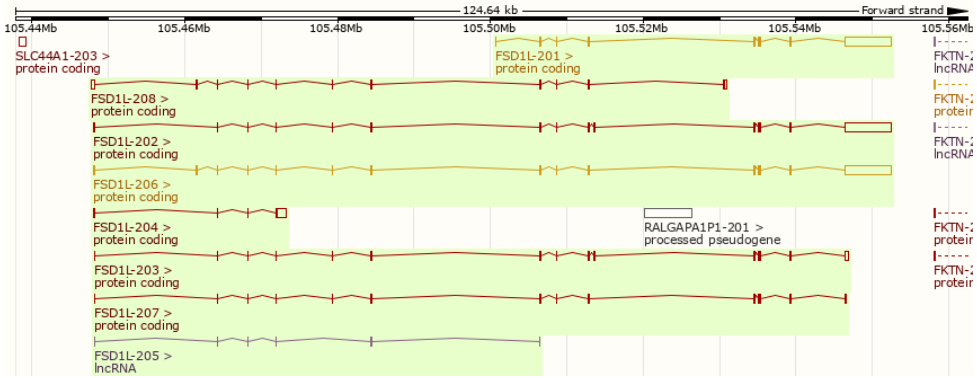


**Figure 19.** *FSD1L* known isoforms from Ensembl (release 98, GRCh38.p13)

Isoform amplification performed on control fibroblasts and total brain extracts showed an increased expression of isoforms 207 and 208 in total brain compared to fibroblasts, as well as a slight increase of isoforms 202 and 203 (Figure 20). Isoform 205, which has recently reported to be a long noncoding RNA (lncRNA), was not expressed in adult control fibroblasts and total brain extract. Unfortunately, isoform 201 did not show the expected amplicon dimension, suggesting that the observed amplicon was an unspecific product.

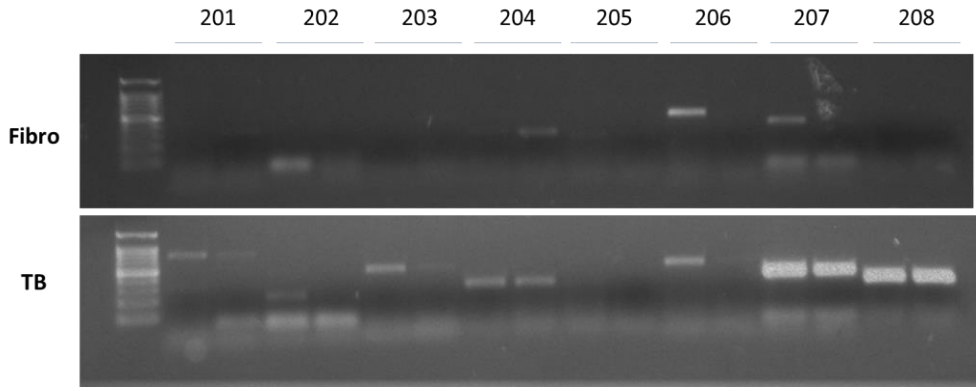


**Figure 20.** *FSD1L* isoforms expression in different tissues (Fibroblasts and

total brain, TB).

The same approach has been adopted for patients' fibroblasts. Interestingly, isoform 203 was present only in patients' fibroblasts and absent in control fibroblasts (Figure 21). Isoform 204 was present in patients' fibroblasts, despite primers were designed within the region containing the variant, suggesting that splicing was not affected in this isoform.

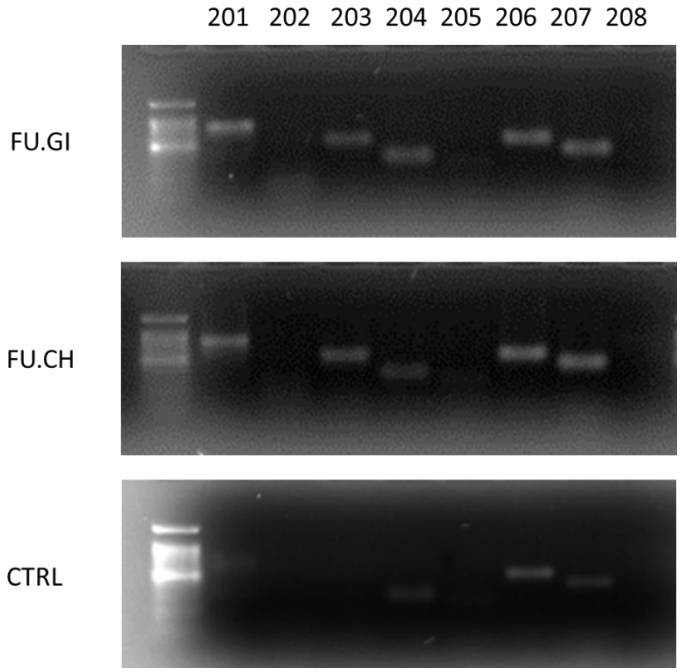


**Figure 21.** *FSD1L* isoforms expression in patients' fibroblasts compared to a control.

I obtained RNA samples from iPSCs, which have been committed towards cerebellar differentiation, at various differentiation steps (T0, T8, T16, T24, and T31). Isoform amplification showed an increased expression of isoforms 203 and 207 at T8, the first decreased rapidly while the second decreased at later stages (T31). Isoform 208 was increased at T24 to decrease again at the final step (T31) (Figure 22). At late differentiation time (T31), a slight increased expression of isoform 204 was observed. Interestingly, isoform 205 (the lncRNA) was present at each differentiation time, as well as isoform 206.

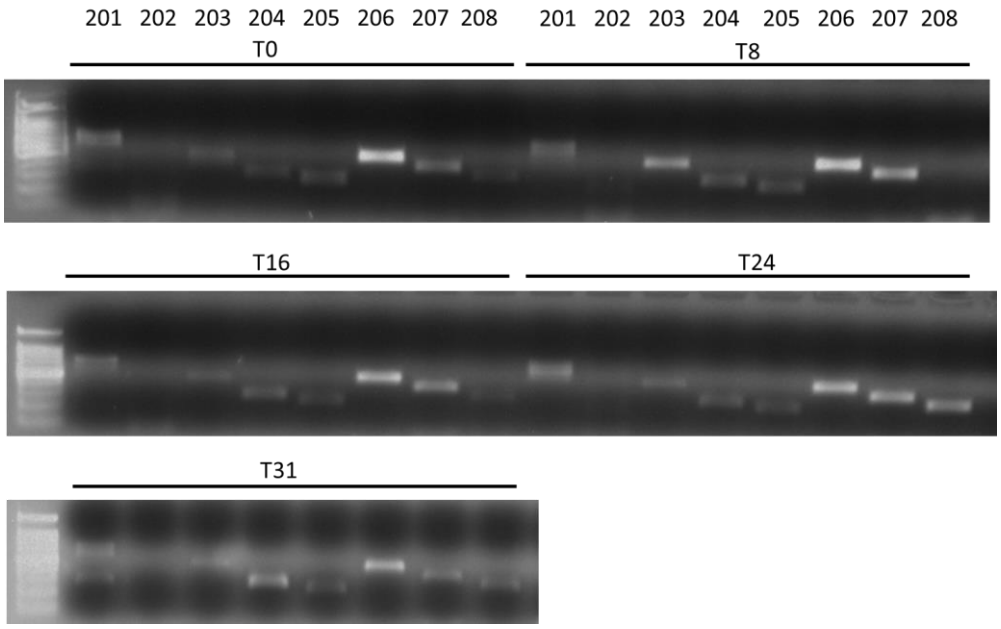


**Figure 22.** *FSD1L* isoforms expression in iPSCs toward a cerebellar differentiation at different times.

# 6. Discussion

This thesis is part of two research projects funded by the Italian Ministry of Health and European Research Council and aimed at improving the genetic characterization of CBCDs and to identify new candidate genes. I assessed the frequency of pathogenic variants in known genes in a big cohort of CBCDs patients by a Custom Target Resequencing approach strategy. Pathogenic variants have been identified in 59% probands with Joubert Syndrome and 67% with Pontocerebellar Hypoplasia. Despite the existence of a European founder variant p.(Ala307Ser) in the *TSEN54* gene, the most frequently mutated gene was *CASK,* accounting for up to 35% of cases (considering both SNVs and CNVs), while the *TSEN54* founder variant has been identified in just 16% of cases. Among the other CBCDs analyzed, the most interesting finding was the *de novo SPTBN2* variant (c.1438C>T, p.Arg480Trp) in a child with a severe congenital form of cerebellar ataxia. Heterozygous pathogenic variant in this gene are usually responsible for a form of spinocerebellar ataxia (SCA5), a progressive autosomal dominant disorder with adult onset. Otherwise, homozygous variants have been associated with an autosomal recessive form of early onset spinocerebellar ataxia (SCAR14). The illustrated case highlights the complexity of monogenic disorders because a phenotype that resembles SCAR14, typically associated with homozygous pathogenic variants, here is associated to a *de novo* occurrence of a variant in the heterozygous state (Nuovo et al. 2018).

Indeed, this is the third case described with this specific de novo variant, further corroborating the hypothesis of a gain-of-function pathogenic mechanism.

Using the data obtained for the Joubert Syndrome, it has been possible to estimate its overall prevalence of 0.47 per 100,000 population, for the first time in Italy. When considering only pediatric age, JS prevalence has been estimated in 1.7 per 100,000.

Whole Exome Sequencing allowed identifying new candidate genes for CBCDs and expanding the phenotypic expression of several other genes.

*SUFU*, the first gene identified by WES, was found mutated in two siblings with mild Joubert Syndrome characteristics. This gene is a suppressor of the Sonic Hedgehog pathway, an important molecular mechanism that regulates the embryonic development, particularly of limbs and CNS. Constitutive knock-out mouse model for *Sufu* is lethal (Svard et al. 2006), while conditional KO leads to polydactyly (Zhulyn et al. 2014; Zhulyn et al. 2015) and alteration of brainstem and cerebellum (Kim et al. 2011). Moreover, a knock-in mouse for a missense variant in *Sufu* showed cranio-facial defects and polydactyly (Makino et al. 2015). All these features are compatible with the clinical and neuroradiological findings in the two siblings with the p.(Ile406Thr) variant in *SUFU*. Functional studies on patients' fibroblasts showed a decreased protein stability, supporting the negative impact of this variantfor the regulation of the SHH pathway (De Mori et al. 2017).

The *GSX2* variant p.(Gln251Arg) is located in the DNA binding domain

of this transcription factor, while the p.(Ser9*) variant leads to early protein truncation. *GSX2* is involved in the regulation of the embryonic neuronal development and a knock-out mouse model for *Gsh2* was characterized by missing olfactory tubercle and striatal size reduction (Toresson et al. 2000). These alterations are comparable to the morphological abnormalities of the *GSX2* patients with putamen and globus pallidus agenesis, hypothalamus-mesencephalic fusion and olfactory bulbs hypoplasia. Functional studies on patient's fibroblasts demonstrated a decreased protein expression and a reduced nuclear localization compared to control fibroblasts (De Mori et al. 2019).

The *TTL* p.(Cys338Tyr) variant identified with WES analysis was an excellent candidate since the neuroimaging phenotype in the two sisters with this variantclosely resembled that observed in patients with pathogenic variants in any of the Tubulin family genes, and the *TTL* gene encodes for a Tubulin-Tyrosine Ligase, an enzyme which is essential for tubulin tyrosination. The variant was predicted to be deleterious from most of the *in silico* prediction tools and the amino acid position resulted to be highly conserved. *TTL* is a cytosolic enzyme involved in the posttranslational modification of alpha-tubulin. Alpha-tubulin within assembled microtubules is detyrosinated over time at the C terminus. After microtubule disassembly, *TTL* restores the tyrosine residues and consequently participates in a cycle of tubulin detyrosination and tyrosination (Erck et al. 2003). Microtubules have an essential role in cytoarchitecture, cell motility, vesicle and organelle transport and cell division. Moreover, tubulin genes are

highly expressed during brain development and have great importance for the correct neurogenesis and neuron migration. Pathogenic variants in these genes are responsible for a wide range of overlapping Malformations of Cortical Development (MCDs) which are defined “Tubulinopathies” (Romaniello et al. 2018). It has been described a Ttl-null mouse model with defective breathing and ataxia which died within 24 hours after birth. The brain of mutant mice showed disorganization of neuronal networks, including disruption of the corticothalamic loop. Cultured Ttl-null neurons also displayed morphogenetic anomalies, including accelerated and erratic neurite outgrowth and premature axonal differentiation (Erck et al. 2005). Given these evidences, *TTL* could be considered a possible novel gene causing a form of tubulinopathy with cerebellar involvement. Functional studies on patients’ fibroblasts are still ongoing.

The *de novo* truncating variant p.(Ala164Asnfs*13) in *IRF2BPL* has been identified in a child with a complex neurodegenerative disease with the peculiar finding of lysosomal storage at electron microscopy examination on skin biopsy. The *IRF2BPL* gene is ubiquitously expressed in human tissues, including central nervous system, and is highly intolerant to loss of function variants (pLI=0.96, o/e=0.11, GnomAD database). The identified deletion would result in a prematurely truncated protein, lacking many functional domains including three PEST sequences and the nuclear localization signal, possibly resulting in reduced degradation and mislocalization of the mutant protein (Rampazzo et al. 2000). The biological function of

*IRF2BPL* is still unknown but evidence suggests that it acts as a transcriptional activator and may also function as an E3 ubiquitin ligase in the ubiquitin proteasome pathway in Wnt signalling (Heger et al. 2007; Higashimori et al. 2018). At the time of the WES analysis, the gene was not yet associated to a human disease, but two cases with a comparable phenotype were described on the Undiagnosed Disease Network database. Very recently, a functional study on Drosophila has shown that a complete loss of the *IRF2BPL* orthologue is lethal early in development, whereas partial knockdown with RNA interference in neurons leads to neurodegeneration (Marcogliese et al. 2018). Moreover, this study reported five additional patients with *de novo* variants in *IRF2BPL* affected by a similar neurodegenerative disease. Nevertheless, no association with Lysosomal Storage Disorders has been yet performed as this is the first case of *IRF2BPL* variant with the evidence of lysosomal deposits.

WES analysis allowed to identify the *KIF1A* p.(Arg307Gln) pathogenic variant with *de novo* occurrence, in a boy with cerebellar atrophy and in presence of axonal spheroids in peripheral nervous system; these findings suggested the diagnosis of Infantile Neuroaxonal Dystrophy (INAD), a neurodegenerative disorder often caused by pathogenic variants in the *PLA2G6* gene. *KIF1A* encodes for a motor protein involved in the anterograde transport of synaptic-vesicle precursors along axons. Variants in *KIF1A* are associated with a spectrum of neurological disorders, including an autosomal dominant form of mental retardation, hereditary sensory neuropathy and a recessive

form of spastic paraplegia. This evidence contributes to further expand the phenotypic spectrum associated to *KIF1A* pathogenic variants and confirms the complexity of Mendelian disorders, given the phenotypic variability due to alterations in the same gene.

WES of two brothers with Nonprogressive congenital ataxia and cerebellar atrophy showed the presence of the two compound heterozygous variants p.(Val214Glyfs*189) and p.(Thr465Thr) in *BRAT1.* Biallelic pathogenic variants in *BRAT1* are mainly associated with a rare disease, lethal in the neonatal age, known as "Rigidity and Multifocal Seizure Syndrome" (RMFSL). This syndrome is characterized by microcephaly, rigidity, drug-resistant focal seizures, apnea and bradycardia. Magnetic resonance may be normal or show a spectrum of alterations ranging from frontal hypoplasia to cerebro-cerebellar atrophy. To date, 24 patients with pathogenic variants in this gene have been described, but only 20 of them belong to the RMFSL phenotype. The remaining cases present variable clinical, neuroradiological and electroencephalographic (EEG) manifestations, defining a heterogeneous group of *BRAT1*-related neurodevelopmental disorders. A single family with variants in the *BRAT1* gene associated with nonprogressive cerebellar ataxia and psychomotor retardation in absence of epilepsy or EEG abnormalities has been reported in the literature (Srivastava et al. 2016). This description overlaps with the clinical phenotype of our patient. The presented data demonstrate how *BRAT1*-related disorders constitute a variable phenotypic spectrum ranging from severe RMFSLs to mild

forms of nonprogressive pediatric ataxia. The synonymous variant p.(Thr465Thr) was located at the last nucleotide of the exon and this often implies an alteration on the splicing mechanism. This assumption was confirmed by the cDNA analysis which showed an exclusion of the exon containing the synonymous variant. The resulting transcript, however, presented an alteration of the reading frame, resulting in a premature stop codon after 23 amino acids. Minigene assay is ongoing with the aim to observe whether there is a quote of transcript which escape the altered splicing, explaining the milder phenotype of the two brothers compared to the lethal phenotype associated with *BRAT1* pathogenic variants.

The sequencing of cDNA from patients' fibroblasts with the *FSD1L* variant p.(Leu137Val) revealed the presence of an exonic cryptic splice site caused by this variant. Isoform amplification in different tissues showed a differential expression of some isoforms. Two isoforms (207 and 208) were highly expressed in the brain tissue, suggesting an important role for this protein in the central nervous system. Unlike control fibroblasts, patients' cells presented the expression of isoform 203, which was present in brain tissue. This finding could be explained by an effect on isoform expression caused by the variant in *FSD1L*. Nevertheless, the variant did not affect the isoform 204 that was present in patients' fibroblasts, since the nucleotide change is located at the last exon of this isoform and this is probably the reason why splicing is not affected. Interestingly, *FSD1L* isoforms have a differential expression in the cerebellar differentiation

process. This time-lapse analysis revealed a constant presence of isoform 206, a transient increased expression of isoform 203 (T8). Increased expression at T8 also for isoform 207 that gradually decreased at later steps. A transient expression of isoform 208 at T24 and a slight increase of isoform 204 at T31. Strikingly, the lncRNA (isoform 205) was always present, suggesting that this molecule may have a role in cellular differentiation, at least toward cerebellar differentiation.

*FSD1L* is not yet associated to a human disease. It is highly expressed in brain and has a microtubule-binding activity. It contains a coiled coil domain, followed by a Fibronectin type 3 domain and a C-terminal B30.2 box (that is the microtubule-binding site). All these domains have protein-protein binding activity and evidence suggest that *FSD1L* may act as an oligomeric protein (Stein et al. 2002). Interestingly, the deletion identified in the family described here falls in the coiled coil domain, suggesting that it may affects the protein-protein interaction. Mutated patients had neurodevelopmental delay, intellectual disability, seizures, optic atrophy, spastic tetraparesis, thin corpus callosum and mild ventricular dilatation. *FSD1L* has sequence similarity with *MID1*, which alterations are responsible for the Opitz GBBB syndrome. This X-linked disorder is characterized by facial anomalies, genitourinary abnormalities and laryngo-tracheo-esophageal defects. Developmental delay, intellectual disability and midline brain defects (Dandy-Walker malformation and agenesis or hypoplasia of the corpus callosum and/or cerebellar vermis) are also described (Meroni 1993).

*FSD1L* has been submitted to Gene Matcher and other two families with variants in this gene have been recruited. Generation of a *FSD1L* KO mouse model is ongoing by one of the two groups contacted. The first mouse embryo analyzed showed ventricular dilatation, abnormalities of callosum fibers and neuronal migration abnormalities.

# 7. Conclusions and perspectives

The advent of Next Generation Sequencing allowed to analyze a big number of genes simultaneously. This technological progress represented a big step forward for the understanding of genetic bases of CBCDs, given the genetic heterogeneity and the phenotypic overlapping of these disorders. Moreover, the possibility to sequence many genes in a time is less time- and cost-consuming with respect to sequence each gene individually. A genetic diagnosis for CBCDs is important as it can give information concerning the disease such as recurrence risk and outcome. Moreover, it holds great importance for prenatal diagnosis and preimplantation genetic diagnosis. Despite Custom Target Resequencing is a good approach for screening of known genes, there is still a portion of CBCDs without a genetic diagnosis, suggesting the presence of still uncovered genes. To solve this issue, Whole Exome Sequencing represents a good strategy to identify new candidate genes and to expand the current knowledge of CBCDs.

DNA analysis does not allow the identification of hidden alterations, for instance deep intronic variants which unlikely affect transcript processing or exonic synonymous variant that may create a cryptic splice site. These alterations could be identified through transcriptome analysis, a NGS technique performed on RNA samples that allows to identify new transcripts or altered isoforms.

Moreover, CNV analysis with NGS, although possible, requires a complex bioinformatic analysis and not always is reliable. For this reason, a high resolution Custom CGH Array could be a good approach for the detection of genomic rearrangement.

# References

**Agamy O, Ben Zeev B, Lev D, Marcus B, Fine D, Su D, Narkis G, Ofir R, Hoffmann C, Leshinsky-Silver E, Flusser H, Sivan S, Soll D, Lerman-Sagie T and Birk OS**. Mutations disrupting selenocysteine formation cause progressive cerebello-cerebral atrophy. Am J Hum Genet. 2010;87:538-544

**Barkovich AJ, Millen KJ and Dobyns WB**. A developmental and genetic classification for midbrain-hindbrain malformations. Brain. 2009;132:3199-3230

**Bertini E, Zanni G and Boltshauser E**. Nonprogressive congenital ataxias. Handb Clin Neurol. 2018;155:91-103

**Bosemani T, Orman G, Boltshauser E, Tekes A, Huisman TA and Poretti A**. Congenital abnormalities of the posterior fossa. Radiographics. 2015;35:200-220

**De Mori R, Romani M, D'Arrigo S, Zaki MS, Lorefice E, Tardivo S, Biagini T, Stanley V, Musaev D, Fluss J, Micalizzi A, Nuovo S, Illi B, Chiapparini L, Di Marcotullio L, et al.** Hypomorphic Recessive Variants in SUFU Impair the Sonic Hedgehog Pathway and Cause Joubert Syndrome with Cranio-facial and Skeletal Defects. Am J Hum Genet. 2017;101:552-563

**De Mori R, Severino M, Mancardi MM, Anello D, Tardivo S, Biagini T, Capra V, Casella A, Cereda C, Copeland BR, Gagliardi S, Gamucci A, Ginevrino M, Illi B, Lorefice E, et al.** Agenesis of the putamen and globus pallidus caused by recessive mutations in the homeobox gene GSX2. Brain. 2019;

**Dines JN, Liu YJ, Neufeld-Kaiser W, Sawyer T, Ishak GE, Tully HM, Racobaldo M, Sanchez-Valle A, Disteche CM, Juusola J, Torti E, McWalter K, Doherty D and Dipple KM**. Expanding phenotype with

severe midline brain anomalies and missense variant supports a causal role for FOXA2 in 20p11.2 deletion syndrome. Am J Med Genet A. 2019;179:1783-1790

**Doherty D, Millen KJ and Barkovich AJ**. Midbrain and hindbrain malformations: advances in clinical diagnosis, imaging, and genetics. Lancet Neurol. 2013;12:381-393

**Erck C, MacLeod RA and Wehland J**. Cloning and genomic organization of the TTL gene on mouse chromosome 2 and human chromosome 2q13. Cytogenet Genome Res. 2003;101:47-53

**Erck C, Peris L, Andrieux A, Meissirel C, Gruber AD, Vernet M, Schweitzer A, Saoudi Y, Pointu H, Bosc C, Salin PA, Job D and Wehland J**. A vital role of tubulin-tyrosine-ligase for neuronal organization. Proc Natl Acad Sci U S A. 2005;102:7853-7858

**Forzano F, Mansour S, Ierullo A, Homfray T and Thilaganathan B**. Posterior fossa malformation in fetuses: a report of 56 further cases and a review of the literature. Prenat Diagn. 2007;27:495-501

**Grinberg I, Northrup H, Ardinger H, Prasad C, Dobyns WB and Millen KJ**. Heterozygous deletion of the linked genes ZIC1 and ZIC4 is involved in Dandy-Walker malformation. Nat Genet. 2004;36:1053-1055

**Guemez-Gamboa A, Caglayan AO, Stanley V, Gregor A, Zaki MS, Saleem SN, Musaev D, McEvoy-Venneri J, Belandres D, Akizu N, Silhavy JL, Schroth J, Rosti RO, Copeland B, Lewis SM, et al.** Loss of Protocadherin-12 Leads to Diencephalic-Mesencephalic Junction Dysplasia Syndrome. Ann Neurol. 2018;84:638-647

**Heger S, Mastronardi C, Dissen GA, Lomniczi A, Cabrera R, Roth CL, Jung H, Galimi F, Sippell W and Ojeda SR**. Enhanced at puberty 1 (EAP1) is a new transcriptional regulator of the female neuroendocrine reproductive axis. J Clin Invest. 2007;117:2145-2154

**Higashimori A, Dong Y, Zhang Y, Kang W, Nakatsu G, Ng SSM, Arakawa T, Sung JJY, Chan FKL and Yu J**. Forkhead Box F2 Suppresses Gastric Cancer through a Novel FOXF2-IRF2BPL-beta-Catenin Signaling Axis. Cancer Res. 2018;78:1643-1656

**Howley MM, Keppler-Noreuil KM, Cunniff CM, Browne ML and National Birth Defects Prevention S**. Descriptive epidemiology of cerebellar hypoplasia in the National Birth Defects Prevention Study. Birth Defects Res. 2018;110:1419-1432

**Jissendi-Tchofo P, Severino M, Nguema-Edzang B, Toure C, Soto Ares G and Barkovich AJ**. Update on neuroimaging phenotypes of mid-hindbrain malformations. Neuroradiology. 2015;57:113-138

**Kim JJ, Gill PS, Rotin L, van Eede M, Henkelman RM, Hui CC and Rosenblum ND**. Suppressor of fused controls mid-hindbrain patterning and cerebellar morphogenesis via GLI3 repressor. J Neurosci. 2011;31:1825-1836

**Makino S, Zhulyn O, Mo R, Puviindran V, Zhang X, Murata T, Fukumura R, Ishitsuka Y, Kotaki H, Matsumaru D, Ishii S, Hui CC and Gondo Y**. T396I mutation of mouse Sufu reduces the stability and activity of Gli3 repressor. PLoS One. 2015;10:e0119455

**Marcogliese PC, Shashi V, Spillmann RC, Stong N, Rosenfeld JA, Koenig MK, Martinez-Agosto JA, Herzog M, Chen AH, Dickson PI, Lin HJ, Vera MU, Salamon N, Graham JM, Jr., Ortiz D, et al.** IRF2BPL Is Associated with Neurological Phenotypes. Am J Hum Genet. 2018;103:456

**Matthijs G, Schollen E, Pardon E, Veiga-Da-Cunha M, Jaeken J, Cassiman JJ and Van Schaftingen E**. Mutations in PMM2, a phosphomannomutase gene on chromosome 16p13, in carbohydrate-deficient glycoprotein type I syndrome (Jaeken syndrome). Nat Genet. 1997;16:88-92

**Meroni G**. X-Linked Opitz G/BBB Syndrome. GeneReviews((R)).

1993;

**Mitchison HM and Valente EM**. Motile and non-motile cilia in human pathology: from function to phenotypes. J Pathol. 2017;241:294-309

**Namavar Y, Barth PG, Poll-The BT and Baas F**. Classification, diagnosis and potential mechanisms in pontocerebellar hypoplasia. Orphanet J Rare Dis. 2011;6:50

**Nuovo S, Micalizzi A, D'Arrigo S, Ginevrino M, Biagini T, Mazza T and Valente EM**. Between SCA5 and SCAR14: delineation of the SPTBN2 p.R480W-associated phenotype. Eur J Hum Genet. 2018;26:928-929

**Pinchefsky EF, Accogli A, Shevell MI, Saint-Martin C and Srour M**. Developmental outcomes in children with congenital cerebellar malformations. Dev Med Child Neurol. 2019;61:350-358

**Poretti A, Boltshauser E and Huisman TA**. Cerebellar and Brainstem Malformations. Neuroimaging Clin N Am. 2016;26:341-357

**Rampazzo A, Pivotto F, Occhi G, Tiso N, Bortoluzzi S, Rowen L, Hood L, Nava A and Danieli GA**. Characterization of C14orf4, a novel intronless human gene containing a polyglutamine repeat, mapped to the ARVD1 critical region. Biochem Biophys Res Commun. 2000;278:766-774

**Romani M, Micalizzi A and Valente EM**. Joubert syndrome: congenital cerebellar ataxia with the molar tooth. Lancet Neurol. 2013;12:894-905

**Romaniello R, Arrigoni F, Fry AE, Bassi MT, Rees MI, Borgatti R, Pilz DT and Cushion TD**. Tubulin genes and malformations of cortical development. Eur J Med Genet. 2018;61:744-754

**Santoro M, Coi A, Barisic I, Garne E, Addor MC, Bergman JEH, Bianchi F, Boban L, Braz P, Cavero-Carbonell C, Gatt M, Haeusler**

**M, Kinsner-Ovaskainen A, Klungsoyr K, Kurinczuk JJ, et al.** Epidemiology of Dandy-Walker Malformation in Europe: A EUROCAT Population-Based Registry Study. Neuroepidemiology. 2019;1-11

**Sellick GS, Barker KT, Stolte-Dijkstra I, Fleischmann C, Coleman RJ, Garrett C, Gloyn AL, Edghill EL, Hattersley AT, Wellauer PK, Goodwin G and Houlston RS**. Mutations in PTF1A cause pancreatic and cerebellar agenesis. Nat Genet. 2004;36:1301-1305

**Severino M, Tortora D, Pistorio A, Ramenghi LA, Napoli F, Mancardi MM, Striano P, Capra V and Rossi A**. Expanding the spectrum of congenital anomalies of the diencephalic-mesencephalic junction. Neuroradiology. 2016;58:33-44

**Srivastava S, Olson HE, Cohen JS, Gubbels CS, Lincoln S, Davis BT, Shahmirzadi L, Gupta S, Picker J, Yu TW, Miller DT, Soul JS, Poretti A and Naidu S**. BRAT1 mutations present with a spectrum of clinical severity. Am J Med Genet A. 2016;170:2265-2273

**Stein PA, Toret CP, Salic AN, Rolls MM and Rapoport TA**. A novel centrosome-associated protein with affinity for microtubules. J Cell Sci. 2002;115:3389-3402

**Svard J, Heby-Henricson K, Persson-Lek M, Rozell B, Lauth M, Bergstrom A, Ericson J, Toftgard R and Teglund S**. Genetic elimination of Suppressor of fused reveals an essential repressor function in the mammalian Hedgehog signaling pathway. Dev Cell. 2006;10:187-197

**Toresson H, Potter SS and Campbell K**. Genetic control of dorsal-ventral identity in the telencephalon: opposing roles for Pax6 and Gsh2. Development. 2000;127:4361-4371

**Zaki MS, Saleem SN, Dobyns WB, Barkovich AJ, Bartsch H, Dale AM, Ashtari M, Akizu N, Gleeson JG and Grijalvo-Perez AM**. Diencephalic-mesencephalic junction dysplasia: a novel recessive brain malformation. Brain. 2012;135:2416-2427

**Zanni G and Bertini E**. X-linked ataxias. Handb Clin Neurol. 2018;155:175-189

**Zhulyn O, Li D, Deimling S, Vakili NA, Mo R, Puviindran V, Chen MH, Chuang PT, Hopyan S and Hui CC**. A switch from low to high Shh activity regulates establishment of limb progenitors and signaling centers. Dev Cell. 2014;29:241-249

**Zhulyn O and Hui CC**. Sufu and Kif7 in limb patterning and development. Dev Dyn. 2015;244:468-478

# *Supplementary tables*

**Supplementary table 1.** CCM panel gene list with associated phenotype

| Gene | Phenotype |
|---|---|
| **EXOSC3** | PCH |
| **VRK1** | PCH |
| **TSEN54** | PCH |
| **TSEN34** | PCH |
| **TSEN2** | PCH |
| **CASK** | PCH |
| **RARS2** | PCH |
| **TOE1** | PCH |
| **CHMP1A** | PCH |
| **AMPD2** | PCH |
| **SEPSECS** | PCH |
| **PTF1A** | Pancreatic and cerebellar agenesis |
| **ROBO3** | Horizontal gaze palsy with progressive scoliosis (HGPPS) |
| **VLDLR** | Cerebellar hypoplasia and mental retardation with or without quadrupedal locomotion 1 |
| **ARHGEF2** | Neurodevelopmental disorder with midbrain and hindbrain malformations |
| **PMM2** | Congenital disorder of glycosylation, type Ia (CDG1a) |
| **ZIC1** | DWM |
| **ZIC4** | DWM |
| **FOXC1** | DWM |
| **LAMC1** | DWM |
| **AP1S2** | DWM associated with Pettigrew syndrome |
| **NID1** | DWM |
| **WDR81** | Cerebellar ataxia, mental retardation, and dysequilibrium syndrome 2 (CAMRQ2) |

| | |
|---|---|
| **SIL1** | Cerebellar ataxia (Marinesco-Sjogren syndrome) |
| **ATP2B3** | Spinocerebellar ataxia, X-linked 1 |
| **OPHN1** | Mental retardation, X-linked, with cerebellar hypoplasia and distinctive facial appearance |
| **CAMTA1** | Cerebellar ataxia, nonprogressive, with mental retardation |
| **GRM1** | Spinocerebellar ataxia, autosomal recessive 13 |
| **CA8** | Cerebellar ataxia and mental retardation with or without quadrupedal locomotion 3 |
| **KIAA0226** | Spinocerebellar ataxia, autosomal recessive 15 |
| **KIAA0196** | NPCA associated with Ritscher-Schinzel syndrome, DWM-like malformation |
| **ABCB7** | Anemia, sideroblastic, with ataxia |
| **PAX6** | Gillespie-like syndrome |
| **ATP8A2** | NPCA, mental retardation, and dysequilibrium syndrome 4 |
| **ATCAY** | Cayman cerebellar ataxia |
| **ZNF592** | Spinocerebellar ataxia, autosomal recessive 5 |
| **GPSM2** | Chudley-McCullough syndrome, cerebellar dysplasia |
| **DKC1** | Hoyeraal-Hreidarsson syndrome, dyskeratosis congenita with cerebellar hypoplasia |
| **SPTBN2** | Spinocerebellar ataxia, autosomal recessive 14 |
| **GRID2** | Spinocerebellar ataxia, autosomal recessive 18 |
| **ADCK3** | CoQ10 deficiency (NPCA described) |

**Supplementary table 2**. JS panel gene list with associated phenotype

| Gene | Phenotype/Protein Function |
|---|---|
| **AHI1** | Joubert syndrome 3 |
| **ARL13B** | Joubert syndrome 8 |
| **B9D1** | Joubert syndrome 27 |
| **B9D2** | Joubert syndrome 34 |

| | |
|---|---|
| **C2CD3** | Orofaciodigital syndrome XIV |
| **C5ORF42** | Joubert syndrome 17 |
| **CC2D2A** | Joubert syndrome 9 |
| **CEP290** | Joubert syndrome 5 |
| **CEP41** | Joubert syndrome 15 |
| **CSPP1** | Joubert syndrome 21 |
| **EXOC8** | Bardet-Biedl Syndrome 18; Cargo trafficking to the periciliary membrane; a family with JS (Dixon-Salazar TJ 2012) |
| **IFT172** | Short-rib thoracic dysplasia 10 with or without polydactyly, associated with vermis hypoplasia; three JS patients (Bachmann-Gagescu et al 2015a, Halbritter et al 2013) |
| **INPP5E** | Joubert syndrome 1 |
| **KIAA0586** | Joubert syndrome 23 |
| **KIF7** | Joubert syndrome 12 |
| **MKS1** | Joubert syndrome 28 |
| **NPHP1** | Joubert syndrome 4 |
| **OFD1** | Joubert syndrome 10 |
| **PDE6D** | Joubert syndrome 22 |
| **POC1B** | Cone-rod dystrophy 20; protein involved in ciliogenesis; a JS family (Beck 2014) |
| **RPGRIP1L** | Joubert syndrome 7 |
| **TCTN1** | Joubert syndrome 13 |
| **TCTN2** | Joubert syndrome 24 |
| **TCTN3** | Joubert syndrome 18 |
| **TMEM138** | Joubert syndrome 16 |
| **TMEM216** | Joubert syndrome 2 |
| **TMEM231** | Joubert syndrome 20 |
| **TMEM237** | Joubert syndrome 14 |
| **TMEM67** | Joubert syndrome 6 |
| **TTC21B** | Nephronophthisis 12; three patients with JS (Davis 2011) |
| **ZNF423** | Joubert syndrome 19 |
| **NPHP4** | Nephronophthisis 4; protein required for building functional cilia |

| | |
|---|---|
| **TMEM17** | Orofaciodigital Syndrome VI and Meckel Syndrome, Type 1; protein localized at the transition zone of primary cilia |
| **KIAA0556** | Joubert syndrome 26 |
| **CEP120** | Joubert syndrome 31 |
| **CEP104** | Joubert syndrome 25 |
| **SUFU** | Joubert syndrome 32 |
| **GLI3** | Polydactyly, Postaxial, Type A1; Regulator of Shh ciliar pathway |
| **KIF14** | Meckel syndrome 12 |
| **NPHP3** | Meckel syndrome 7 |
| **PIBF1** | Joubert syndrome 33 |
| **TMEM218** | Orofaciodigital Syndrome Vi and Meckel Syndrome, Type 1; protein involved in ciliogenesis and function |
| **INVS** | Nephronophthisis 2, infantile; interactor of NPHP1 |
| **CEP164** | Nephronophthisis 15; protein required for primary cilia assembly |
| **CROCC** | Major structural component of the ciliary rootlet, a cytoskeletal-like structure in ciliated cells |
| **TMEM80** | Orofaciodigital Syndrome Vi and Meckel Syndrome, Type 1; protein located at the ciliary transition zone |
| **SLITRK4** | It is involved in synaptogenesis and promotes synapse differentiation |
| **KIAA0753** | Orofaciodigital syndrome XV; two JS siblings with growth hormone deficiency (Stephen J 2017) |
| **TMEM107** | Joubert syndrome 29 |
| **DDX59** | Orofaciodigital syndrome V |
| **SCLT1** | Nephronophthisis 15; Orofaciodigital Syndrome IX (Adly 2013) |
| **TBC1D32** | Required for high-level Shh responses in the developing neural tube; Orofaciodigital Syndrome IX (Adly 2013) |
| **INTU** | Orofaciodigital syndrome XVII; regulation of cilia formation, interaction with C5orf42 (Toriyama 2016) |
| **WDPCP** | Bardet-Biedl syndrome 15, interaction with C5orf42 (Toriyama 2016) |

**Supplementary table 3.** List of pathogenic variants identified in JS probands

| Sample | Gene | Pathogenic Variant |
|---|---|---|
| **NG523** | AHI1 | c.1123A>C, p.(T375P)/c.1997A>T/P.(D666V) |
| **NG708** | AHI1 | c.2168G>A, p.(R723Q)/c.2168G>A, p.(R723Q) |
| **NG1660** | AHI1 | c.682_684delGACinsTAA, p.(D228*)/c.1918G>T, p.(E640*) |
| **NG1701** | AHI1 | c.1328T>A, p.(V443D) |
| **NG1838** | AHI1 | c.2687A>G, p.(H896R) |
| **NG1760** | AHI1 | c.1500C>G, p.(Y500*)/chr6:135751067-135756077del |
| **NG1788** | AHI1 | c.1981T>C, p.(S661P) |
| **NG2041** | AHI1 | c.1484G>T, p.(R495L)/c.2033C>A, p.(A678D) |
| **NG2052** | AHI1 | c.2493-1G>A |
| **NG2085** | AHI1 | c.1550G>A, p.(W517*) |
| **NG2171** | AHI1 | c.2266+1G>A/c.1828C>T, p.(R610*) |
| **NG2194** | AHI1 | c.1780-1G>C/c.1912+1G>A |
| **NG2212** | AHI1 | c.640G>T, p.(E214*) |
| **NG2317** | AHI1 | c.985C>T, p.(R329*) |
| **NG2329** | AHI1 | c.2687A>G p.(H896R) |
| **NG2409** | AHI1 | c.787dupC, p.(Q263Pfs*7) |
| **NG3012** | AHI1 | c.1474T>C, p.(S492P)/c.2156A>C, p.(D719A) |
| **NG3537** | AHI1 | c.1213A>C, p.(T405P) |
| **NG3959** | AHI1 | c.931G>A, p.(V311I)/c.1151G>C, p.(S384T) |
| **NG3975** | AHI1 | c.1829G>C, p.(R610P)/c.2671C>T, p.(R891*) |
| **NG3573** | AHI1 | c.1779+1G>A |
| **NG4167** | AHI1 | c.2105C>T, p.(T702M)/c.2167C>G, p.(R723G) |
| **NG4175** | AHI1 | c.2687A>G, p.(H896R) |
| **NG4331** | AHI1 | c.985C>T, p.(R329*)/c.1550G>A, p.(W517*) |
| **NG4340** | AHI1 | c.2009T>C, p.(L670P)/c.2687A>G, p.(H896R) |
| **NG4711** | AHI1 | c.2273A>C, p.(H758P) |
| **NG4761** | AHI1 | c.1328T>A, (p.V443D) |
| **NG4891** | AHI1 | c.2168G>A, p.(R723Q) |
| **NG5829** | AHI1 | c.910dupA, p.(T304Nfs*6) |
| **NG3480** | B9D1 | c.95A>G, p.(Y32C)/c.520_522delGTG, p.(V174del) |
| **NG3561** | B9D1 | c.467G>A, p.(R156Q) |
| **NG3637** | B9D1 | c.467G>A, p.(R156Q)/c.511_513TTC, p.(F171del) |
| **NG729** | C5orf42 | c.1819delT, p.(Y607Tfs*6)/c.8406_8407delGT, p.(F2803Sfs*14) |

| | | |
|---|---|---|
| **NG1613** | C5orf42 | c.3868T>C, p.(S1290P)/c.7477C>T, p.(R2493*) |
| **NG1610** | C5orf42 | c.3551G>A, p.(R1184H)/c.4034A>G, p.(Q1345R) |
| **NG1692** | C5orf42 | c.4168_4177delCTCAGACACTinsGTTG, (p.L1390_C1393delinsVG)/c.1214C>T p.(A405V) |
| **NG1827** | C5orf42 | c.3550C>T, p.(R1184C)/c.7429C>T, p.(Q2477*) |
| **NG1956** | C5orf42 | c.7988_7989delGA, p.(G2663Afs*39) |
| **NG1972** | C5orf42 | c.1784T>G,p.(L595*), c.4796C>A,p.(T1599K)/c.4634G>A, p.(R1545H) |
| **NG1717** | C5orf42 | c.4394_4397dup, p.(E2870*)/c.8608G>T, p.(D1467Rfs*7) |
| **NG1755** | C5orf42 | c.493delA,p.(I165Yfs*16)/c.8608G>T, p.(E2870*) |
| **NG1784** | C5orf42 | c.7988_7989delGA, (p.G2663Afs*39) |
| **NG1795** | C5orf42 | c.493delA, p.(I165Yfs*16)/c.817A>C, p.(N273H) |
| **NG1804** | C5orf42 | c.817A>C, (p.N273H)/c.3091T>C, (p.S1031P) |
| **NG1810** | C5orf42 | c.3998C>T,p.(P1333L) |
| **NG2050** | C5orf42 | c.3012T>A, p.(Y1004*)/c.8406_8407delGT, p.(F2803Sfs*14) |
| **NG2058** | C5orf42 | c.3545delA, p.(N1182Ifs*25)/c.8406_8407delGT, p.(F2803Sfs*13) |
| **NG2075** | C5orf42 | c.5348C>A, p.(A1783D)/c.5733T>G, p.(Y1911*) |
| **NG2137** | C5orf42 | c.493delA, p.(I165Yfs*16)/c.4643A>G, p.(D1548G) |
| **NG2149** | C5orf42 | c.493delA, p.(I165Yfs*16)/c.968C>T, p.(T323M) |
| **NG2163** | C5orf42 | c.7477C>T, p.(R2493*) |
| **NG2218** | C5orf42 | c.2123_2124delAA, p.(E708Gfs*6)/c.8810C>G, p.(S2937*) |
| **NG2274** | C5orf42 | c.7234-2_7234delAGT/c.8406_8407delGT, p.(F2910Sfs*13) |
| **NG2295** | C5orf42 | c.2624C>T, p.(S875F)/c.5733T>G, p.(Y1911*) |
| **NG2301** | C5orf42 | c.2641C>T, p.(L881F)/c.7817T>A, p.(L2606*) |
| **NG2401** | C5orf42 | c.7400+1G>A |
| **NG3154** | C5orf42 | c.3380C>T, p.(S1127L) |
| **NG3157** | C5orf42 | c.143G>A, p.(G48E)/c.1784T>G, p.(L595*) |
| **NG3488** | C5orf42 | c.7477C>T, p.(R2493*)/c.3854G>A, p.(R1286H) |
| **NG3548** | C5orf42 | c.455C>T, p.(S152F)/c.2334G>A, p.(W778*) |
| **NG3674** | C5orf42 | c.3599C>T, p.(A1200V)/c.7817T>A, p.(L2606*) |
| **NG3831** | C5orf42 | c.7477C>T, p.(R2493*)/c.7477C>T, (p.R2493*) |
| **NG4544** | C5orf42 | c.3820A>G, p.(R1274G)/c.3190C>G, p.(P1064A) |
| **NG4713** | C5orf42 | c.4634G>A, p.(R1545H)/c.4634G>A, p.(R1545H) |
| **NG4734** | C5orf42 | c.1784T>G, p.(L595*)/c.8884C>T, p.(R2962*) |
| **NG4834** | C5orf42 | c.3577C>T, p.(R1193C)/c.493delA, p.(I165Yfs*16) |
| **NG4896** | C5orf42 | c.5348C>A, (p.A1783D)/c.1041_1044dupGCTA, p.(T349Afs*26) |

| | | |
|---|---|---|
| **NG5208** | C5orf42 | c.1819delT, p.(Y607Tfs*6), c.7817T>A, p.(L2606*)/c.8263dupA, p.(T2755Nfs*8) |
| **NG5022** | C5orf42 | c.1819delT, p.(Y607Tfs*6)/c.5348C>A, p.(A1783D) |
| **NG5214** | C5orf42 | c.5594dupA, p.(N1865Kfs*3)/c.3380C>T, p.(S1127L) |
| **NG5245** | C5orf42 | c.1819delT, p.(Y607Tfs*6), c.7817T>A p.(L2606*)/c.2933G>A, p.(R978Q) |
| **NG5847** | C5orf42 | c.4634G>A, p.(R1545H) |
| **NG5881** | C5orf42 | c.260T>G, p.(L87R)/c.1036G>A, p.(E346K) |
| **NG518** | CC2D2A | c.4669T>A, p.(Y1557N) |
| **NG1817** | CC2D2A | c.3289delG, p.(V1097Ff*1)/c.4667A>T, p.(D1556V) |
| **NG1690** | CC2D2A | c.4256delG, p.(G1420Dfs*8)/c.4667A>T p.(D1556V) |
| **NG1835** | CC2D2A | c.4136T>C, p.(L1379P)/c.4667A>T, p.(D1556V) |
| **NG1895** | CC2D2A | c.1252C>G, p.(H418D)/c.2999A>T, p.(E1000V) |
| **NG1729** | CC2D2A | c.4597_4598delCT, p.(L1533Vfs*11)/c.4667A>T, p.(D1556V) |
| **NG1761** | CC2D2A | c.2991_2996delAAGAAG, p.(E998_E999del)/c.3544T>C, p.(W1182R) |
| **NG2066** | CC2D2A | c.3364C>T, p.(P1122S) |
| **NG2108** | CC2D2A | c.3452T>C, p.(V1151A)/c.4147G>C, p.(A1383P) |
| **NG2136** | CC2D2A | c.1017+1G>A/c.4667A>T, p.(D1556V) |
| **NG2222** | CC2D2A | c.3341C>T, p.(T1114M)/c.4220A>G, p.(Y1407C) |
| **NG2307** | CC2D2A | c.2993_2998delAAGAAG, p.(E999_E1000del)/c.3289delG, p.(V1097Ffs*2) |
| **NG2361** | CC2D2A | c.3195delG, p.(Q1065Hfs*33)/c.4465G>C, p.(D1489H) |
| **NG2547** | CC2D2A | c.3856T>C, p.(C1286R) |
| **NG2793** | CC2D2A | c.2848C>T, (p.R950*) |
| **NG3161** | CC2D2A | c.4786G>A, p.(A1596T) |
| **NG3389** | CC2D2A | c.2999A>T, p.(E1000V)/c.3638delG, p.(G1213Afs*7) |
| **NG3359** | CC2D2A | c.3364C>T, p.(P1122S) |
| **NG3962** | CC2D2A | c.1558C>T, p.(R520*)/c.4345C>A, p.(P1449T) |
| **NG4096** | CC2D2A | c.3347C>T, p.(T1116M)/c.4582C>T, p.(R1528C) |
| **NG4395** | CC2D2A | c.2848C>T, p.(R950*) |
| **NG4520** | CC2D2A | c.4667A>T, p.(D1556V)/c.4842_4845delCTCT, p.(S1615Lfs*16) |
| **NG4768** | CC2D2A | c.3596T>C, p.(I1199T)/c.4102C>A, p.(H1368N) |
| **NG5262** | CC2D2A | c.879dupA, (p.V294Sfs*5)/c.4258C>A, p.(Q1420K) |
| **NG5347** | CC2D2A | c.4289T>C, p.(V1430A)/c.4774G>T, p.(E1592*) |
| **NG3696** | CC2D2A | c.4256delG, p.(G1419Dfs*9)/c.4667A>T, p.(D1556V) |
| **NG5528** | CC2D2A | c.3289delG, p.(V1097Ffs*2)/c.4667A>T, p.(D1556V) |
| **NG5685** | CC2D2A | c.3084delG, p.(K1028Rfs*3)/c.4455C>A, p.(Y1485*) |
| **NG5716** | CC2D2A | c.2999A>T, (p.E1000V)/c.3084delG p.(Y1029Rfs*3) |

| | | |
|---|---|---|
| **NG5809** | CC2D2A | c.3976-2A>G/c.4667A>T, (p.D1556V) |
| **NG3024** | CEP104 | c.1485+1G>A |
| **NG3245** | CEP104 | c.375_376delT, p.(Y126NFs*1) |
| **NG3908** | CEP120 | c.581T>C, p.(V194A) |
| **NG5485** | CEP120 | c.2179G>C p.(A727P)/c.2917C>T, p.(R973*) |
| **NG326** | CEP290 | c.5493delA, p.(A1832Pfs*19)/del EX42-54 |
| **NG507** | CEP290 | c.2086delA, p.(D696Mfs*5)/c.5668G>T, p.(G1890*) |
| **NG510** | CEP290 | c.3811C>T, p.(R1271*)/c.5734_5735delTG, p.(W1912Gfs*4) |
| **NG1450** | CEP290 | c.21G>T, p.(W7C) |
| **NG1430** | CEP290 | c.4732G>T,p.(E1578*) |
| **NG1495** | CEP290 | c.4393C>T, p.(R1465*)/c.4723A>T, p.(K1575*) |
| **NG1725** | CEP290 | c.5668G>T, p.(G1890*) |
| **NG1892** | CEP290 | c.5163delT, p.(R1721fs*2) |
| **NG1893** | CEP290 | c.4882C>T, p.(Q1628*)/c.5941G>T, p.(E1981*) |
| **NG1322** | CEP290 | c.3175dupA, p.(I1059Nfs*11) |
| **NG1995** | CEP290 | c.3814C>T, p.(R1272*)/c.1683delA, p.(Q561fs*12) |
| **NG1754** | CEP290 | c.5668G>T, p.(G1890*)/c.5431_5433delGA, p.(N1810fs*6) |
| **NG2043** | CEP290 | c.6031C>T, p.(R2011*)/c.1657_1666delA, p.(L552fs*20) |
| **NG2077** | CEP290 | c.4882C>T, p.(Q1628*) |
| **NG2120** | CEP290 | c.1823A>G, p.(K608R)/c.3894dupT, p.(L1299fs*) |
| **NG2256** | CEP290 | c.5493delA, p.(A1832Pfs*18)/c.7341dupA, p.(L2448Tfs*7) |
| **NG2319** | CEP290 | c.2368-1G>A/c.5709+2T>G |
| **NG3049** | CEP290 | c.5995-5999delGATAT, p.(D1999Ifs*23) |
| **NG3130** | CEP290 | c.5668G>T, p.(G1890*) |
| **NG3180** | CEP290 | c.2086delA, p.(D696Mfs*5)/c.1666delA, p.(I556Ffs*16) |
| **NG3280** | CEP290 | c.2306T>C, p.(I769T)/c.4966G>T, p.(E1656*) |
| **NG3749** | CEP290 | c.3573+1G>T/c.4771C>T, p.(Q1591*) |
| **NG3752** | CEP290 | c.5668G>T, p.(G1890*) |
| **NG3815** | CEP290 | c.2722C>T, p.(R908*)/c.7320_7324delCTTAG, p.(L2440Rfs*12) |
| **NG3844** | CEP290 | c.6277delG, p.(V2093Sfs*3) |
| **NG3905** | CEP290 | c.5668G>T, p.(G1890*) |
| **NG4220** | CEP290 | c.4522C>T, p.(R1508*)/c.4394G>A, p.(R1465Q) |
| **NG4322** | CEP290 | c.1078C>T, p.(R360*)/c.6919_6920delGA, p.(E2307Tfs*3) |
| **NG4336** | CEP290 | c.1645C>T, p.(R549*)/c.1666delA, p.(I556Ffs*16) |
| **NG4532** | CEP290 | c.5668G>T, p.(G1890*) |

| | | |
|---|---|---|
| **NG4575** | CEP290 | c.6072C>A, p.(Y2024*) |
| **NG4577** | CEP290 | c.5668G>T, p.(G1890*) |
| **NG5336** | CEP290 | c.4882C>T, p.(Q1628*)/c.6277delG, p.(V2093fs*4) |
| **NG5440** | CEP290 | c.3894dupT, p.(K1299*)/c.5668G>T, p.(G1890*) |
| **NG5682** | CEP290 | c.1987A>T, p.(K663*)/ c.148C>G, p.(H50D) |
| **NG5736** | CEP290 | c.1909+2T>A/c.4763T>G, p.(L1588*) |
| **NG3198** | CEP290 | c.4864C>T, p.(R1622C)+OFD1 c.2608_2609insTCTA, p.(Q870Lfs*1) |
| **NG1314** | CEP41 | c.423-2A>C |
| **NG2406** | CROCC | c.5023C>T, p.(R1675C)/c.5722C>T, p.(R1908C) |
| **NG1565** | CSPP1 | c.432dupT, p.(N145*) |
| **NG1341** | CSPP1 | c.2320C>T, p.(R774*)/c.2953+1G>A |
| **NG2144** | CSPP1 | c.2243_2244delAA, p.(E750Gfs*30)/c.2868delGinsTGT, p.(A957Cfs*11) |
| **NG2229** | CSPP1 | c.658C>T, p.(R220*)/c.950G>A, p.(R317K) |
| **NG2279** | CSPP1 | c.2243_2244delAA, p.(E750Gfs*30) |
| **NG4172** | CSPP1 | c.1214+1G>A/c.2243_2244delAA, p.(E750Gfs*30) |
| **NG4529** | CSPP1 | c.2503_2506delTTGA, p.(I836Gfs*7) |
| **NG4584** | HIP1R | c.1766G>A, p.(R589Q) |
| **NG547** | INPP5E | c.1132C>T, p.(R378C) |
| **NG1447** | INPP5E | c.1132C>T, p.(R378C) |
| **NG1777** | INPP5E | c.1277C>A,p.(T426N) |
| **NG2170** | INPP5E | c.874C>G, p.(R292G)/c.1629C>G, p.(Y543*) |
| **NG2259** | INPP5E | c.907G>A, p.(V303M)/c.1753C>T, p.(R585C) |
| **NG3220** | INPP5E | c.1468G>T, p.(D490Y)/c.1718A>G, p.(Y573C) |
| **NG3924/ NG3803** | INPP5E | c.907G>A, p.(V303M)/c.1264A>G, p.(T422A) |
| **NG4582** | INPP5E | c.1064C>T, p.(T355M) |
| **NG5659** | INPP5E | c.1106_1108dupGCG, p.(G369dup)/c.874C>G, p.(R292G) |
| **NG1485** | KIAA0586 | c.428delG, p.(R143Kfs*4)/c.2209C>T, p.(Arg737*) |
| **NG1936** | KIAA0586 | c.428delG, p.(R143K*4)/chr14:58,910,526-58,917,507del |
| **NG1775** | KIAA0586 | c.428delG, p.(R143Kfs*4)/c.863_864del, p.(Q288Rfs*7) |
| **NG2286** | KIAA0586 | c.428delG, p.(R143Kfs*4)/c.1815G>A, p.(Q605Q) |
| **NG2326** | KIAA0586 | c.428delG, p.(R143Kfs*4)/c.863_864del, p.(Q288Rfs*7) |
| **NG2458** | KIAA0586 | c.428delG, p.(R143Kfs*4)/c.1658_1661delinsAAA, p.(V553Efs*79) |
| **NG2548** | KIAA0586 | c.428delG, p.(R143Kfs*4)/c.3040C>T, p.(Q1014*) |
| **NG2872** | KIAA0586 | c.482delG, p.(R143Kfs*4) |
| **NG3501** | KIAA0586 | c.482delG, p.(R143Kfs*4)/c.1413-1G>C |

| | | |
|---|---|---|
| **NG3516** | KIAA0586 | c.74del, p.(K25Rfs*6) |
| **NG3758** | KIAA0586 | c.428delG, p.(R143Kfs*4)/c.3462delA, p.(G1155Efs*40) |
| **NG4158** | KIAA0586 | c.428delG, p.(R143Kfs*4)/c.649C>T, p.(Q217*) |
| **NG3928** | KIAA0586 | c.428delG, p.(R143Kfs*4)/c.1006C>T, p.(Q336*) |
| **NG4902** | KIAA0586 | c.428delG, p.(R143Kfs*4) |
| **NG5324** | KIAA0586 | c.428delG, p.(R143Kfs*4)/c.1006C>T, p.(Q336*) |
| **NG5253** | KIAA0586 | c.428delG, p.(Arg143Kfs*4)/c.790_793delCTTA, p.(L264Vfs*36) |
| **NG2446** | KIF7 | c.2335G>T, p.(E779*) |
| **NG4243** | KIF7 | c.434A>C, p.(Y145S) |
| **NG4578** | KIF7 | c.2473G>T, p.(E825*) |
| **NG5432** | KIF7 | c.62G>A, p.(R21Q) |
| **NG5914** | KIF7 | c.2896_2897delGC, p.(A966Pfs*81) |
| **NG3358** | MKS1 | c.1461-2A>G |
| **NG3370** | MKS1 | c.240G>T, p.(Y80C)/c.1408-7_1408-35del29 |
| **NG4154** | MKS1 | c.1085_1087delCCT, p.(S362del)/c.1558+1G>T |
| **NG4168** | MKS1 | c.770_771delAT, p.(N257Sfs*36)/c.1446T>G, p.(C482W) |
| **NG4396** | MKS1 | c.1085_1087delCCT, p.(S362del) |
| **NG4506** | MKS1 | c.1399_1407+4delTCCTTCAAGGTGA |
| **NG4851** | MKS1 | c.1476T>G, p.(C492W)/c.340C>T, p.(R114*) |
| **NG5313** | MKS1 | c.378T>A, p.(F126L)/c.805T>C, p.(S269P) |
| **NG5422** | MKS1 | c.1115_1117delCCT, p.(S372del) |
| **NG5540** | MKS1 | c.1476T>G (p.C492W), c.1388G>A (p.R463Q)/c.1600C>T (p.Arg534*) |
| **NG5603** | MKS1 | c.1408-34_1408-6del/c.1476T>G, p.(C492W) |
| **NG3985** | NPHP1 | c.84_87delTTCT,p.(S27Rfs*4) |
| **NG539** | NPHP4 | c.1804C>T, p.(Q602*)/c.452+1G>T |
| **NG4418** | NPHP4 | c.1972C>T, p.(R658*)/c.688A>G, p.(K230E) |
| **NG1488** | OFD1 | c.517+4_517+7delTAAT |
| **NG1557** | OFD1 | c.92G>T, p.(G31V) |
| **NG2296** | OFD1 | c.2315dupT, p.(P772Tfs*4) |
| **NG2386** | OFD1 | c.2488+5 G>T |
| **NG3025** | OFD1 | c.2757+1G>A |
| **NG4325** | OFD1 | c.2725C>T, (p.R909*) |
| **NG5257** | OFD1 | c.710dupA, p.(A238Vfs*2) |
| **NG711** | RPGRIP1L | c.1975delT, p.(S659Lfs*40)/c.1843A>C, p.(T615P) |
| **NG1612** | RPGRIP1L | c.2267delT, (p.I756kfs*14) |
| **NG1317** | RPGRIP1L | c.1843A>C, p.(T615P) |
| **NG1710** | RPGRIP1L | c.2451C>A, p.(Y817*)/c.1843A>C, p.(T615P) |
| **NG1736** | RPGRIP1L | c.1829A>C, p.(H610P) |

| | | |
|---|---|---|
| **NG1766** | RPGRIP1L | c.881A>G, p.(E294G)/c.986_987delAA, p.(K329Tfs*8) |
| **NG1792** | RPGRIP1L | c.1649A>G, p.(Q550R) |
| **NG2224** | RPGRIP1L | c.1649A>G, p.(Q550R) |
| **NG2266** | RPGRIP1L | c.2050C>T, p.(Q684*)/c.2304+1G>T |
| **NG3984** | RPGRIP1L | c.287G>A, p.(G96D)/c.3548C>G, p.(1183A>G) |
| **NG4797** | RPGRIP1L | c.1804C>T, p.(R602*) |
| **NG5503** | RPGRIP1L | c.1843A>C, p.(T615P) |
| **NG1741** | SLITRK4 | c.2495C>G, p.(T832R) |
| **NG3227** | SLITRK4 | c.2478G>C, p.(Q826H) |
| **NG1452** | TCTN1 | c.262G>A, p.(D88N)/c.1718_1721delTTTG, p.(V592Dfs*106) |
| **NG2105** | TCTN1 | c.290G>T, p.(C97F)/c.898C>T, p.(R300*) |
| **NG2579** | TCTN2 | c.1235-1G>A |
| **NG1991** | TCTN3 | c.940G>A, p.(G314R) |
| **NG4462** | TMEM138 | c.380C>T, p.(A127V) |
| **NG1927** | TMEM17 | c.306C>A, p.(N102K) |
| **NG306** | TMEM216 | c.218G>T, p.(R73L) |
| **NG1824** | TMEM216 | c.35G>T, p.(R12L) |
| **NG1349** | TMEM216 | c.218G>T, p.(R73L) |
| **NG2775** | TMEM216 | c.35G>T, p.(R12L) |
| **NG2800** | TMEM216 | c.35G>T, p.(R12L) |
| **NG4752** | TMEM231 | c.269A>C, p.(N90T) |
| **NG514** | TMEM237 | c.52C>T, p.(R18*)/c.553+1G>T |
| **NG1969** | TMEM237 | c.1066dupC, p.(Q356Pfs*23) |
| **NG4574** | TMEM237 | c.151C>T, p.(R51*) |
| **NG5542** | TMEM237 | c.1066_1067insC, p.(Q356Pfs*24)/c.1074G>T, (p.W358C) |
| **NG1413** | TMEM67 | c.577delA, (p.T193qfs*29)/c.1769T>C, p.(F590S) |
| **NG1505** | TMEM67 | c.1115C>A, p.(T372K)/c.2345A>G, p.(H782R) |
| **NG1604** | TMEM67 | c.370G>A, p.(E124K)/c.1073C>T, p.(P358L) |
| **NG1698** | TMEM67 | c.389C>G, p.(P130R)/c.675G>A, p.(W225*) |
| **NG1940** | TMEM67 | c.G1319A, p.(R440Q)/c.2182A>G, p.(S728G) |
| **NG1983** | TMEM67 | c.2439+5G>C |
| **NG1998** | TMEM67 | c.651+2T>G/c.1634G>A, p.(G545E) |
| **NG2016** | TMEM67 | c.1706G>A,p.G569D/c.1860+1G>A |
| **NG2038** | TMEM67 | c.1285C>T, p.(Q429*)/c.1847C>T, p.(A616V) |
| **NG2237** | TMEM67 | c.312+5G>A/p.(I833T) |
| **NG2358** | TMEM67 | c.2216 T>G, p.(L739R)/c.1115C>A, p.(T372K) |
| **NG2367** | TMEM67 | c.1079_1080delCA, p.(T360Rfs*18)/c.1769T>C, p.(F590S) |
| **NG2466** | TMEM67 | c.903C>G, p.(D301E)/c.1538A>G, p.(Y513C) |

| | | |
|---|---|---|
| **NG2473** | TMEM67 | c.769A>G, p.(M257V) |
| **NG2511** | TMEM67 | c.270T>G, p.(N90K)/c.755T>C, p.(M252T) |
| **NG2515** | TMEM67 | c.300C>A, p.(C100*)/c.2498 T>C, p.(I833T) |
| **NG2837** | TMEM67 | c.652-9T>A |
| **NG2865** | TMEM67 | c.619C>T, p.(R207C)/c.1607T>A, p.(V536D) |
| **NG3390** | TMEM67 | c.2086C>T, p.(L696F) |
| **NG3410** | TMEM67 | c.224G>A, p.(G75E)/c.725A>G, p.(N242S) |
| **NG4455** | TMEM67 | c.1843T>C, p.(C615R)/c.2907+1G>A |
| **NG4859** | TMEM67 | c.226A>G, p.(T76A) |
| **NG4954** | TMEM67 | c.755T>C, p.(M252T)/c.1769T>C, p.(F590S) |
| **NG5386** | TMEM67 | c.1843T>C, p.(C615R)/c.579delA, p.(G195Dfs*27) |
| **NG5443** | TMEM67 | c.1843T>C, p.(C615R)/c.1975C>T, p.(Arg659*) |
| **NG5453** | TMEM67 | c.1927C>T, p.(R643*)/c.2086C>T, p.(L696F) |
| **NG5802** | TMEM67 | c.515G>A, p.(R172Q)/c.1321C>T, p.(R441C) |
| **NG2334** | TTC21B | c.985G>A, p.(E329K)/c.3340C>T, p.(Q1114*) |
| **NG4593** | TTC21B | c.626C>T, p.(P209L) |

**Supplementary table 4.** List of pathogenic variants identified in PCH probands

| Sample | Pathogenic Variant |
|---|---|
| **NG2413** | CASK c.2207-2208insGTGTTTTCCTAAGACTAGTG, p.(L737CfsTer8) |
| **NG2513** | CASK c.316C>T, (p.R106*) |
| **NG2659** | CASK c.1610delG, p.(R537Qfs*80) |
| **NG2747** | CASK c.996_997insT, p.(E333*) |
| **NG2868** | CASK c.372_373delGA, p.(Q124Hfs*10 ) |
| **NG2958** | CASK c.82C>T, p.(R28*) |
| **NG3285** | CASK c.1501-1502insA (p.M501Nfs*9) |
| **NG3721** | CASK c.2302+1G>A |
| **NG4042** | CASK c.2446G>T, p.(E816*) |
| **NG4474** | CASK c.1970G>A, p.(W657*) |
| **NG4885** | CASK c.2174_2176delAAG, p.(E725del) |
| **NG5203** | CASK c.2221+1delGinsAT |
| **CCM531** | CASK c.846C>G p.(Y282*) |
| **CCM532** | CASK c.1015+1G>A |
| **NG5730** | CASK c.149C>A, p.(S50*) |
| **NG2512** | CASK dup EX2 |
| **NG3313** | CASK del EX6 |
| **NG5511** | CASK del EX23-27 |
| **NG4882** | CASK del EX4-EX5 |
| **CCM529** | CASK del EX1 |
| **CCM530** | CASK del EX1 |
| **NG5726** | CASK del EX3 |
| **NG3922** | CASK del EX9-EX10 |
| **NG3175** | TSEN54 c.919G>T, p.(A307S) |
| **NG3504** | TSEN54 c.919G>T, p.(A307S) |
| **NG3713** | TSEN54 c.919G>T, p.(A307S) |
| **NG4187** | TSEN54 c.919G>T, p.(A307S) |
| **NG4303** | TSEN54 c.919G>T, p.(A307S) |
| **NG4738** | TSEN54 c.919G>T, p.(A307S) |
| **CCM516** | TSEN54 c.919G>T, p.(A307S) |

| | |
|---|---|
| **CCM517** | TSEN54 c.919G>T, p.(A307S) |
| **NG5158** | TSEN54 c.919G>T, p.(A307S) |
| **NG5303** | TSEN54 c.919G>T, p.(A307S) |
| **NG3212** | EXOSC3 c.395A>C, p.(D132A)/c.545A>T, p.(D182V) |
| **NG4234** | EXOSC3 c.294_303del, p.(99fs*11)/c.395A>C, p.(D132A) |
| **NG3333** | EXOSC3 c.92G>C, p.(G31A) |
| **NG5139** | PMM2 c.368G>A, p.(R123Q)/c.640G>A, p.(G214S); ATP2B3 c.2197G>A, p.(G733R) |
| **NG3821** | RARS2 c.1A>G, p.(M1V)/c.1327T>C/p.(S443P) |
| **NG4005** | VLDLR c.1256G>A, p.(C419Y) |
| **NG3729** | TOE1 c.658G>A, p.(E220K) |

**Supplementary table 5.** List of pathogenic variants identified in other CBCDs

| Sample | Pathogenic Variant | Phenotype |
|---|---|---|
| **NG2082** | LAMA1 c.1404_1405delAG, p.(G469Afs*5)/c.4715_4717dupGTG, p.(G1572dup)/c.4663+1G>C | PBS |
| **NG2421** | LAMA1 c.2616delG, p.(L872Nfs*23)/c.2935delA, p.(R979Gfs*45) | PBS |
| **NG2910** | LAMA1 c.164A>T, p.(H55L)/c.2108C>T, p.(A703V) | PBS |
| **NG3613** | LAMA1 c.2935delA, p.(Arg979Glyfs*45) | PBS |
| **NG3670** | LAMA1 c.2935delA, p.(R979Gfs*45) | PBS |
| **NG4523** | LAMA1 c.184C>T, p.(R62*)/c.1404_1405del, p.(G469Afs*4) | PBS |
| **NG4678** | LAMA1 c.2935delA, p.(R979Gfs*45) | PBS |
| **NG4841** | LAMA1 c.2935delA, p.(R979Gfs*45) | PBS |
| **NG4862** | LAMA1 c.8761C>T, p.(R2921*)/delEX62-EX63 (Real-Time) | PBS |
| **NG4865** | LAMA1 c.2935delA, p.(R979Gfs*45) | PBS |
| **NG4866** | LAMA1 c.8556+1G>A | PBS |
| **NG4867** | LAMA1 c.1774_1775insTTCATAAT, p.(S592Ffs*9)/c.6348dupT; p.(K2117*) | PBS |
| **NG4868** | LAMA1 c.4676delA, p.(E1559Gfs*3)/c.7180C>T, p.(R2394*) | PBS |
| **NG5093** | LAMA1 c.470C>G, p.(S157*)/c.4383_4663del, p.(F1462Lfs*1) | PBS |
| **NG4280** | ROBO3 c.569C>G; p.(P190R)/c.1451G>A, p.(W484*) | HGPPS |
| **NG4783** | ROBO3 c.2108G>C, p.(R703P) | HGPPS |
| **NG2745** | PMM2 c.124G>A, p.(G42R)/c.713G>A, p.(R238H) | WCH |
| **NG5199** | OPHN1 c.116_127delTAATCAAAGACG, p.(V39_D42del) | WCH |
| **NG2381** | PMM2 c.422G>A, p.(R141H)/c.640G>A, p.(G214S) | NPCA |
| **NG3054** | SPTBN2 c.1438C>T, p.(R480W) | NPCA |

| | | |
|---|---|---|
| **NG2780** | SIL1 c.331C>T, p.(R111*) | Progressive cerebellar atrophy |
| **NG2766** | LAMC1 c.961C>T, p.(P321S) | Cerebellar hypodysplasia |

# *List of original manuscripts*

Nuovo S, Bacigalupo I, **Ginevrino M**, Battini R, Bertini ES, Borgatti R, Casella A, Micalizzi A, Nardella M, Romaniello R, Serpieri V, Zanni G, Valente EM, Vanacore N. Age and sex prevalence estimate of Joubert Syndrome in Italy. Neurology. 2019 [*in press*]

**Ginevrino M**, Battini R, Nuovo S, Simonati A, Micalizzi A, Contaldo I, Serpieri V, Valente EM. A novel IRF2BPL truncating variant is associated with endolysosomal storage. Mol Biol Rep. 2019 Nov 21. doi: 10.1007/s11033-019-05109-7. [Epub ahead of print] PubMed PMID: 31583567.

De Mori R, Severino M, Mancardi MM, Anello D, Tardivo S, Biagini T, Capra V, Casella A, Cereda C, Copeland BR, Gagliardi S, Gamucci A, **Ginevrino M**, Illi B, Lorefice E, Musaev D, Stanley V, Micalizzi A, Gleeson JG, Mazza T, Rossi A, Valente EM. Agenesis of the putamen and globus pallidus caused by recessive mutations in the homeobox gene GSX2. Brain. 2019 Oct 1;142(10):2965-2978. doi: 10.1093/brain/awz247. PubMed PMID: 31412107; PubMed Central PMCID: PMC6776115.

Nuovo S, Micalizzi A, D'Arrigo S, **Ginevrino M,** Biagini T, Mazza T, Valente EM. Between SCA5 and SCAR14: delineation of the SPTBN2 p.R480W-associated phenotype. Eur J Hum Genet. 2018 Jul;26(7):928-929. doi: 10.1038/s41431-018-0158-7. Epub 2018 May 25. PubMed PMID: 29795474; PubMed Central PMCID: PMC6018709.

De Mori R, Romani M, D'Arrigo S, Zaki MS, Lorefice E, Tardivo S, Biagini T, Stanley V, Musaev D, Fluss J, Micalizzi A, Nuovo S, Illi B, Chiapparini L, Di Marcotullio L, Issa MY, Anello D, Casella A,

**Ginevrino M**, Leggins AS, Roosing S, Alfonsi R, Rosati J, Schot R, Mancini GMS, Bertini E, Dobyns WB, Mazza T, Gleeson JG, Valente EM. Hypomorphic Recessive Variants in SUFU Impair the Sonic Hedgehog Pathway and Cause Joubert Syndrome with Cranio-facial and Skeletal Defects. Am J Hum Genet. 2017 Oct 5;101(4):552-563. doi: 10.1016/j.ajhg.2017.08.017. Epub 2017 Sep 28. PubMed PMID: 28965847; PubMed Central PMCID: PMC5630196.

### Manuscripts in preparation

De Mori R, Magiera MM, Tardivo S, Accorsi P, **Ginevrino M**, Bodakuntla S, Nuovo S, Giordano L, Lorefice E, Liserre R, Pinelli L, Biagini T, Micalizzi A, Casella A, Mazza T, Steinmetz MO, Janke C, Valente EM. Autosomal recessive tubulinopathy-like disorder caused by loss of function of the tubulin-modifying enzyme Tubulin Tyrosine Ligase

## Manuscripts from other projects

Besides the object of this thesis, I have contributed to other projects with national and international collaborations. First of all, the genetic characterization of a big cohort of Parkinson's Disease and Dystonia patients from different Movement Disorders' centers. Moreover, I performed the genetic characterization of induced pluripotent stem cells (iPSCs) in collaboration with the Laboratory of Experimental Cardiology for Cell and Molecular Therapy at IRCCS Policlinico San Matteo of Pavia. Finally, I have participated to the collection of a big number of DNA samples for the international project: "COmprehensive Unbiased Risk factor Assessment for Genetics and Environment in

Parkinson‘s Disease” (COURAGE-PD).

## Manuscripts from Movement Disorders projects:

Stamelou M, Petrucci S, **Ginevrino M**, Pons R, Papagiannakis N, Stefanis L, Valente EM. Intrafamilial variability in a polish family harbouring a frameshift THAP1 mutation. J Neurol Sci. 2018 May 15;388:158. doi: 10.1016/j.jns.2018.03.026. Epub 2018 Mar 16. PubMed PMID: 29627013.

**Ginevrino M**, Valente EM. The multiple faces of TOR1A: different inheritance, different phenotype. Brain. 2017 Nov 1;140(11):2764-2767. doi: 10.1093/brain/awx260. PubMed PMID: 29088347.

Petrucci S, Ferrazzano G, **Ginevrino M**, Tolve M, Berardelli I, Berardelli A, Fabbrini G, Valente EM. Genetic Paradoxes in an Italian Family with PARK2 Multiexon Duplication. Mov Disord Clin Pract. 2017 Sep 8;4(6):889-892. doi: 10.1002/mdc3.12531. eCollection 2017 Nov-Dec. PubMed PMID: 30713982; PubMed Central PMCID: PMC6353389.

Marsili L, Suppa A, Di Stasio F, Belvisi D, Upadhyay N, Berardelli I, Pasquini M, Petrucci S, **Ginevrino M**, Fabbrini G, Cardona F, Defazio G, Berardelli A. BDNF and LTP-/LTD-like plasticity of the primary motor cortex in Gilles de la Tourette syndrome. Exp Brain Res. 2017 Mar;235(3):841-850. doi: 10.1007/s00221-016-4847-6. Epub 2016 Nov 30. PubMed PMID: 27900437.

## Manuscripts from collaboration with Laboratory of

Experimental Cardiology for Cell and Molecular Therapy, Fondazione IRCCS Policlinico San Matteo, Pavia

Mura M, Pisano F, Stefanello M, **Ginevrino M**, Boni M, Calabrò F, Crotti L, Valente EM, Schwartz PJ, Brink PA, Gnecchi M. Generation of two human induced pluripotent stem cell (hiPSC) lines from a long QT syndrome South African founder population. Stem Cell Res. 2019 Aug;39:101510. doi: 10.1016/j.scr.2019.101510. Epub 2019 Jul 24. PubMed PMID: 31398660.

Mura M, Lee YK, Pisano F, **Ginevrino M**, Boni M, Calabrò F, Crotti L, Valente EM, Schwartz PJ, Tse HF, Gnecchi M. Generation of the human induced pluripotent stem cell (hiPSC) line PSMi005-A from a patient carrying the KCNQ1-R190W mutation. Stem Cell Res. 2019 May;37:101437. doi: 10.1016/j.scr.2019.101437. Epub 2019 Apr 13. PubMed PMID: 31009818.

Mura M, Lee YK, Pisano F, **Ginevrino M**, Boni M, Calabrò F, Crotti L, Valente EM, Schwartz PJ, Tse HF, Gnecchi M. Generation of the human induced pluripotent stem cell (hiPSC) line PSMi004-A from a carrier of the KCNQ1-R594Q mutation. Stem Cell Res. 2019 May;37:101431. doi: 10.1016/j.scr.2019.101431. Epub 2019 Mar 27. PubMed PMID: 30974404.

Mura M, Pisano F, Stefanello M, **Ginevrino M**, Boni M, Calabrò F, Crotti L, Valente EM, Schwartz PJ, Brink PA, Gnecchi M. Generation of the human induced pluripotent stem cell (hiPSC) line PSMi007-A from a Long QT Syndrome type 1 patient carrier of two common variants in the NOS1AP gene. Stem Cell Res. 2019 Apr;36:101416. doi: 10.1016/j.scr.2019.101416. Epub 2019 Mar 6. PubMed PMID: 30878014.

Mura M, **Ginevrino M**, Zappatore R, Pisano F, Boni M, Castelletti S, Crotti L, Valente EM, Schwartz PJ, Gnecchi M. Generation of the human induced pluripotent stem cell (hiPSC) line PSMi003-A from a patient affected by an autosomal recessive form of Long QT Syndrome type 1. Stem Cell Res. 2018 May;29:170-173. doi: 10.1016/j.scr.2018.04.003. Epub 2018 Apr 6. PubMed PMID: 29684900.

Mura M, Lee YK, **Ginevrino M**, Zappatore R, Pisano F, Boni M, Dagradi F, Crotti L, Valente EM, Schwartz PJ, Tse HF, Gnecchi M. Generation of the human induced pluripotent stem cell (hiPSC) line PSMi002-A from a patient affected by the Jervell and Lange-Nielsen syndrome and carrier of two compound heterozygous mutations on the KCNQ1 gene. Stem Cell Res. 2018 May;29:157-161. doi: 10.1016/j.scr.2018.04.002. Epub 2018 Apr 7. PubMed PMID: 29677589.

## Manuscripts from collaboration in the international project “COmprehensive Unbiased Risk factor Assessment for Genetics and Environment in Parkinson‘s Disease” (COURAGE-PD)

Kishore A, Ashok Kumar Sreelatha A, Sturm M, von-Zweydorf F, Pihlstrøm L, Raimondi F, Russell R, Lichtner P, Banerjee M, Krishnan S, Rajan R, Puthenveedu DK, Chung SJ; International Parkinson's Disease Genomics Consortium (IPDGC); **Comprehensive Unbiased Risk Factor Assessment for Genetics and Environment in Parkinson's Disease (COURAGE-PD)**, Bauer P, Riess O, Gloeckner CJ, Kruger R, Gasser T, Sharma M. Understanding the role of genetic variability in LRRK2 in Indian population. Mov Disord. 2019 Apr;34(4):496-505. doi: 10.1002/mds.27558. Epub 2018 Nov 28.

PubMed PMID: 30485545.

Blauwendraat C, Reed X, Kia DA, Gan-Or Z, Lesage S, Pihlstrøm L, Guerreiro R, Gibbs JR, Sabir M, Ahmed S, Ding J, Alcalay RN, Hassin-Baer S, Pittman AM, Brooks J, Edsall C, Hernandez DG, Chung SJ, Goldwurm S, Toft M, Schulte C, Bras J, Wood NW, Brice A, Morris HR, Scholz SW, Nalls MA, Singleton AB, Cookson MR; **COURAGE-PD (Comprehensive Unbiased Risk Factor Assessment for Genetics and Environment in Parkinson's Disease) Consortium**, the French Parkinson's Disease Consortium, and the International Parkinson's Disease Genomics Consortium (IPDGC). Frequency of Loss of Function Variants in LRRK2 in Parkinson Disease. JAMA Neurol. 2018 Nov 1;75(11):1416-1422. doi: 10.1001/jamaneurol.2018.1885. PubMed PMID: 30039155; PubMed Central PMCID: PMC6248108.

Blauwendraat C, Kia DA, Pihlstrøm L, Gan-Or Z, Lesage S, Gibbs JR, Ding J, Alcalay RN, Hassin-Baer S, Pittman AM, Brooks J, Edsall C, Chung SJ, Goldwurm S, Toft M, Schulte C; International Parkinson's Disease Genomics Consortium (IPDGC), **COURAGE-PD Consortium**, Hernandez D, Singleton AB, Nalls MA, Brice A, Scholz SW, Wood NW. Insufficient evidence for pathogenicity of SNCA His50Gln (H50Q) in Parkinson's disease. Neurobiol Aging. 2018 Apr;64:159.e5-159.e8. doi: 10.1016/j.neurobiolaging.2017.12.012. Epub 2017 Dec 20. PubMed PMID: 29398121; PubMed Central PMCID: PMC5823280.

Blauwendraat C, Faghri F, Pihlstrom L, Geiger JT, Elbaz A, Lesage S, Corvol JC, May P, Nicolas A, Abramzon Y, Murphy NA, Gibbs JR, Ryten M, Ferrari R, Bras J, Guerreiro R, Williams J, Sims R, Lubbe S, Hernandez DG, Mok KY, Robak L, Campbell RH, Rogaeva E, Traynor BJ, Chia R, Chung SJ; International Parkinson's Disease Genomics Consortium (IPDGC), **COURAGE-PD Consortium**, Hardy JA, Brice A, Wood NW, Houlden H, Shulman JM, Morris HR, Gasser T, Krüger

R, Heutink P, Sharma M, Simón-Sánchez J, Nalls MA, Singleton AB, Scholz SW. NeuroChip, an updated version of the NeuroX genotyping platform to rapidly screen for variants associated with neurological diseases. Neurobiol Aging. 2017 Sep;57:247.e9-247.e13. doi: 10.1016/j.neurobiolaging.2017.05.009. Epub 2017 May 17. PubMed PMID: 28602509; PubMed Central PMCID: PMC5534378